Available online at www.CivileJournal.org

Civil Engineering Journal

(E-ISSN: 2476-3055; ISSN: 2676-6957)

Vol. 10, No. 06, June, 2024

Local Scour around Different-Shaped Bridge Piers

Siva K. Reddy [1*], Sruthi T. Kalathil [1], Venu Chandra [1]

[1] *Department of Civil Engineering, Indian Institute of Technology Madras, Chennai 600036, India.*

Received 26 December 2023; Revised 07 May 2024; Accepted 13 May 2024; Published 01 June 2024

Abstract

Local scour around piers is the major cause of bridge failures, and its estimation is critical for safe design. The present study aims to identify a modified pier shape that can reduce local scour compared to a circular pier. In addition, M5 models are developed for maximum scour depth prediction and compared with the existing equations available in the literature. Thus, the effect of pier shape and alignment on local scour is experimentally investigated using three pier models with the same cross-sectional area placed in isolated and tandem arrangements under clear-water conditions. These are circular (M1) and two modified pier shapes (M2 and M3), where M2 is a combination of semi-circle and triangle oriented either way (M2a and M2b), and M3 is a further modification to M2a with a small protrusion on the semi-circular end. The results showed that the local scour depth for aligned (skew angle, $\alpha = 0°$) M2a, M2b, and M3 piers is reduced by 23.5%, 50%, and 55%, respectively, compared to the M1 pier but not if $\alpha > 0°$. In tandem arrangements, the least scour depths observed around M1 and M2a at $X = 1.0D$ (X is clear-spacing between piers and D is pier diameter), and M3 and M1 at $X = 1.75D$ placed as front and rear pier, respectively. It is observed that the developed M5 models are more accurate compared to the existing equations. Flow intensity (V/V_c) and α have more influence on the scour depth prediction around tandem and isolated piers, respectively.

Keywords: Scour Control; Pier Shape; Skewed Piers; Tandem Piers; Scour Depth Prediction; M5 Model.

1. Introduction

Bridges play a significant role in a nation's transportation system. Bridge failures are disastrous events with far-reaching socio-economic impacts. In the United States, 45% of bridge failures were caused by hydraulic events such as extreme floods and local scour [1]. Obstruction to the river flow by a bridge pier causes the development of a horseshoe vortex associated with the downflow on the upstream side and the wake vortices behind the pier due to flow separation. The interaction of the vortex system with the sediment bed causes an increase in the bed shear stresses and sediment removal in the vicinity of the pier, defined as local scour [2–5]. The magnitude of the three-dimensional turbulent flow field lowering the riverbed around a pier indicates the scour depth, which can be influenced by the pier geometry, flow properties, and sediment characteristics [6]. Excess scouring around bridge pier foundations can lead to structural instability and failure. An accurate scour depth estimation of the bridge pier and the proper design of its foundation are important and need to be investigated to safeguard the bridges.

Therefore, research on scouring around bridge piers and techniques for its control has gained much momentum over the past six decades [7–12]. Reducing scour by introducing different control mechanisms and modified pier shapes is necessary for a safe and economical bridge design. The vortex system developed around a pier is the primary mechanism of scouring. The scour mechanism is complex and mainly governed by the pier size, shape, and orientation with approach flow [13–16]. The scour depth on the upstream side is proportional to the pier width exposed to the approach flow [7].

* Corresponding author: ce17d023@smail.iitm.ac.in

http://dx.doi.org/10.28991/CEJ-2024-010-06-019

Bridge piers are categorized into blunt-nosed and streamlined piers, subjected to the stream flow direction. A streamlined pier has a profile aligned with the flow direction, while a blunt-nosed pier disrupts the flow. Chiew [17] and Li & Tao [18] reviewed the effectiveness of various scour countermeasures and reported that streamlined piers could perform well by reducing the downflow, pressure field, and vortex strength [19]. Several countermeasures against scour exist, among which pier-shape modification is considered highly important [10, 12] because the scouring process is influenced by the altered flow pattern and boundary layer formation around the pier [13]. An optimal pier shape minimizes flow disturbance and scour depth [20]. In addition to circular cross-sections, investigations with various geometrical shapes, such as rectangular, airfoil, elliptical, lenticular, hexagonal, streamlined, and sharp-nosed piers, have been studied to understand the shape effect on the flow field and scouring [7, 13, 14, 19, 21, 22]. Among different-shaped piers, literature shows that the rectangular piers experience the highest scour depths, while airfoil-shaped piers exhibit the lowest [13].

The scour depth at an airfoil pier is 50% less than that of a conventional circular pier [3, 7, 23]. Various studies showed a considerable reduction in scour depth due to pier streamlining [14, 19]. The effect of pier shape on scour depth and pier shape factors (K_s) has been discussed by Melville [24], Ettema et al. [25], and Keshavarz et al. [22]. K_s is the ratio between the scour depths of a specific non-circular pier and a circular pier. However, the existing studies considered only conventional shapes such as circular, rectangular, square, triangle, and sharp-nosed piers to investigate the effect of pier shape on scour. Al-Shukur & Obeid [7] reported that estimating scour depth for different-shaped piers is difficult due to the complicated scour mechanism. Based on the literature review, it is evident that further research is necessary to identify an optimum pier shape that can minimize scour depth even further.

The angle of attack, or pier skew angle (α), significantly influences the flow structure and scour depth around bridge piers [26, 27]. Generally, the river migrates, and the flow direction changes temporally at bridge sites, as evident in braided rivers, shifting thalweg in meandering rivers, and river bends [28]. The scour depth rapidly increases around non-circular piers with skew angles due to an increased effective width of the approach flow and complex vortex system [29, 30]. It's important to note that pier shape factors (K_s) are derived when the pier is aligned ($\alpha = 0°$) with the flow [7, 31]. However, Raudkivi [30] and Richardson & Davis [32] suggested that the pier shape effect can be neglected if $\alpha >$ 10°-15°. While streamlined piers are effective in reducing scour depth, their efficiency is limited to axial flow conditions [14, 20, 21, 33, 34, 35]. Streamlined piers, although initially beneficial, lose their effectiveness with increasing skew angles (> 10°-15°) due to their increased projected width, leading to the development of asymmetric scour patterns [9, 31]. Keshavarz et al. [22] investigated the effect of pier shape and angle of attack on scour in a 180° bend and found that pier shape affects the K_s. Ettema et al. [36], Melville [35], and Ahmad et al. [29] used the skew factor (K_α) to account for the impact of skew angle on scour depth around non-circular piers. K_α represents the ratio between the pier scour depths at $\alpha > 0°$ and $\alpha = 0°$. Fenocchi & Natale [37] conducted experiments with rectangular piers of varying aspect ratios and observed an increase in scour depth with increasing α. Ahmad et al. [29] investigated scour around skewed rectangular piers and reported the higher scour depths at $\alpha = 90°$ and the lowest at $\alpha = 0°$. Habib et al. [10] tested the performance of nose-angled piers in scour reduction with α = 0°-30° and found a correlation between increasing α and scour depth. Similarly, a numerical study by Yu & Zhu [38] observed a high degree of sensitivity of scour depth to pier shape and a direct proportionality to α. Habibi et al. [26] investigated the scouring around skewed square piers with α = 0°-30° and proposed a semi-empirical equation for scour depth estimation. However, the existing literature on the skew angle effect is limited to rectangular and square piers [29, 37]. Further exploration is necessary to understand how the skew angles affect the scour depth around other-shaped piers.

Shen et al. [39], Hancu [40], and Sheppard et al. [41] proposed empirical formulae to estimate scour depth, neglecting skew angle and pier shape factor, which are also critical parameters influencing scour depth [5, 14]. However, only a few existing equations consider these factors for estimating the scour depth around various pier shapes [31, 32, 42–44]. These conventional regression-based equations may not capture the non-linearity between the scour depth and the governing parameters [2, 45]. Additionally, accurate scour depth estimation is challenging due to the complicated scour mechanism with the change in pier shape. Abdulkathum et al. [13] developed regression, Gene Expression Programming (GEP), and Artificial Neural Networks (ANN) models for scour depth prediction around different pier shapes and reported the superior accuracy of ANN models. Although the ANN models are accurate, they cannot provide explicit equations for others to use. In contrast, the M5 model effectively captures non-linearity in data and generates simple formulations that can be used by field engineers [45]. Quinlan developed the M5 Model, a decision tree-based regression model [46] that extracts hidden knowledge from data and establishes relationships between the governing parameters [8]. M5 models have recently gained popularity in circular pier scour depth modeling [8, 45, 47]. This study innovates by developing M5 models specifically for predicting the scour depth of various shaped piers.

In bridge construction, piers are often positioned in close proximity in a tandem configuration, either belonging to a single bridge or two parallel bridges. This scenario presents a phenomenon known as pier interference, where the combined scour mechanism at both piers deviates from that of an isolated pier [48, 49]. The flow structure and scour mechanism at tandem piers are more complicated than those at an isolated pier due to the interaction of hydrodynamic flow structures [50–53]. The scour mechanism includes reinforcing, sheltering, vortice shedding, and vortice compression. The reinforcement effect is observed at the tandem piers, and an increase in the scour depth at the upstream pier was reported [36]. The approach flow velocity at the rear pier is reduced and redirected due to the front pier; thus, the rear pier scour depth decreases, described as a sheltering effect [53, 54, 57]. Further, the spacing between the piers (X) placed in tandem influences the scour depth of both piers [49, 53, 55, 57]. Elliott and Baker [56] investigated the effect of pier spacing on scour depth around pier groups and derived empirical equations for scour depth estimation. Ataie-Ashtiani & Beheshti [57] reported that the scour depth of the upstream pier increased until the X was equal to two times the pier size; afterward, it decreased and approached the scour depth of an isolated pier for a higher X. However, Selamoglu [54] observed that the scour depth at the front pier slightly reduced with an increase in X due to the interference of the wake vortices of the front pier and the horseshoe vortex of the rear pier. Khaple et al. [53] noticed that the scour depth decreased up to X, equal to eight times the pier size, but increased with further increases in X. Hassan et al. [48] found that the tandem piers placed at closer spacing had more interference with flow structures. Liu et al. [58] developed a numerical model based on the Reynolds-Averaged Navier-Stokes (RANS) equations, which yielded scour depth results for tandem piers that aligned with the findings of Ataie-Ashtiani & Beheshti [57]. Ravanfar et al. [55] observed a reduction in scour depth at the front pier of non-uniform tandem piers by placing the footing top just below the bed level compared to that of the uniform tandem piers. Further studies are needed to understand the complex scour mechanism of the piers placed in tandem using circular and modified-shaped piers.

The above discussion of the literature indicates that the pier shape and skew angle significantly influence local scour. However, the effect of pier shape and skew angle on scour depth and its modeling have yet to be widely investigated. The objectives of this experimental study are: (i) to investigate the scour around different-shaped isolated piers that are aligned and skewed to the flow direction; (ii) to study the interference effect of tandem piers with different combinations of the pier models and clear-spacing; and (iii) to develop the M5 models to predict the maximum scour depth around different-shaped isolated and tandem bridge piers by using the experimental and literature datasets. For this purpose, a circular and two modified-shaped pier models of equal cross-sectional area, viz. (a) one-half of the pier cross-section is semi-circular and the other is triangular, and (b) a small protrusion is introduced next to the semi-circular portion of the modified pier mentioned in (a), and the triangular portion is unchanged. The experiments were conducted under steady flow and clear-water scour conditions. The scour depths observed for different pier shapes are presented. The accuracy of the developed M5 models is evaluated using statistical indices (R^2, RMSE, and DR) and compared with five widely used equations available in the literature. The developed M5 models are helpful for pier foundation designs in field conditions. This research helps identify the optimum pier shape with minimum scour depth and find the best tandem arrangement among the tested pier models. The following flowchart (Figure 1) describes the steps involved in conducting this study.

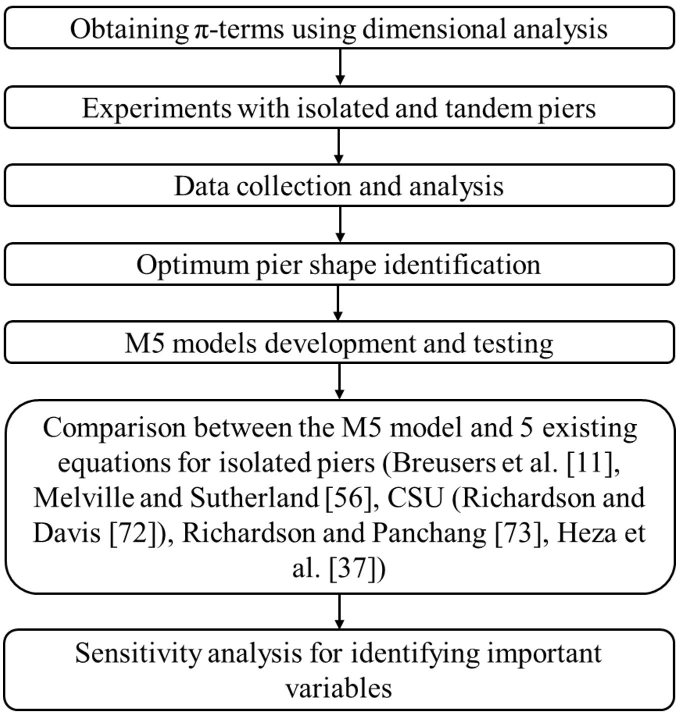

Figure 1. Flowchart of the research methodology

2. Experimental Setup and Methodology

Experiments were carried out in an 8.0 m long, 1.0 m wide, and 1.0 m deep glass-walled flume in the Civil Engineering Department, Indian Institute of Technology Madras, India (Figure 2).

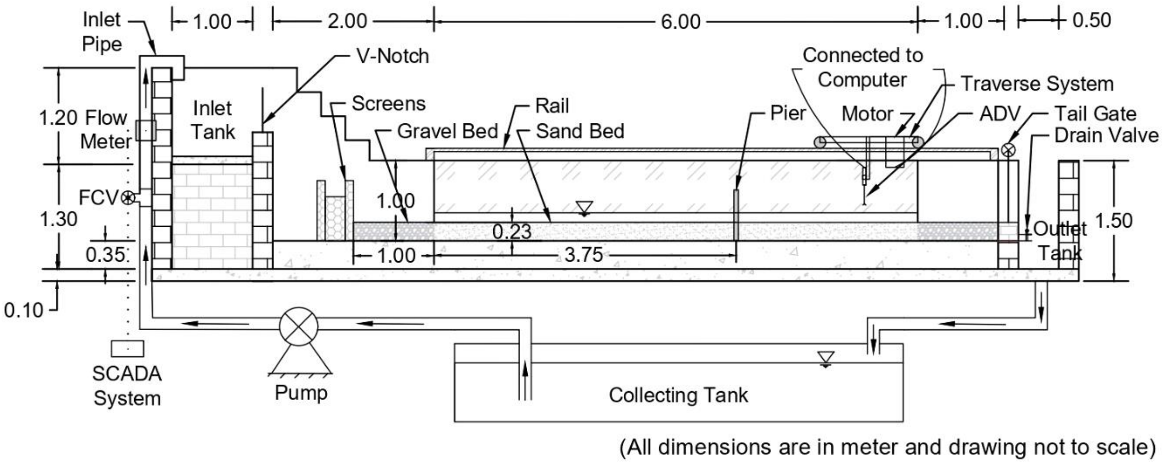

Figure 2. Schematic diagram of the experimental setup

The pier width (D = 5 cm) was fixed, ensuring a flume-to-pier width ratio equal to 20 ($\geq$ 8) to prevent flume boundary interference on the developing scour hole [33]. The flume bed was filled up to a height of 0.23 m with uniform river sand of mean size d_{50} = 0.56 mm, specific gravity S = 2.65, and geometrical standard deviation (σ_g = 1.39) less than 1.4 to minimize the river bed armoring or gradation effects on the scouring [59]. For non-ripple-forming coarse bed material under threshold conditions, the d_{50} must be greater than 0.6 mm [60]. Although the mean sediment size is 0.56 mm, ripples were not observed during the experiments, which may be due to the high σ_g value, and the tests were conducted below the threshold conditions. The longitudinal bed slope (S_o) was maintained at 0.0002. The sediment bed was packed with finer gravel curtains (size = 6 mm) of 1 m on the upstream and downstream ends to still the flow, generate a fully developed turbulent flow within the test section, and prevent undue sediment erosion at the exit, respectively. A 30 HP centrifugal pump continuously recirculated flume water from the sump, maintaining a steady uniform flow. The flow rate (Q) was precisely regulated using the gate valve equipped with a SCADA (Supervisory control and data acquisition) system to maintain steady uniform flow, and it was verified by an electromagnetic flow meter with ± 0.5% accuracy. Flow straighteners (baffle walls and honeycombs) positioned at the flow entrance minimized flow disturbances and promoted uniform flow. A tailgate was used to regulate the flow depth.

2.1. Dimensional Analysis

The influence of pier geometry, flow characteristics, and sediment properties on the scour depth (h_s) at isolated and tandem piers can be expressed as [27, 33-35, 61]:

$$h_s = f\left(D, d_{50}, \sigma_g, h, V, V_c, Sh, Al, L, X, g, \rho, \mu\right) \tag{1}$$

where h_s is maximum scour depth under equilibrium scour conditions, D is pier width, d_{50} is mean sediment size, σ_g is sediment geometrical standard deviation, h is flow depth, V is mean flow velocity, V_c is critical flow velocity for sediment motion, Sh is pier shape effect (= K_s), Al is pier alignment effect (= α), L is the pier length, X is clear spacing between tandem piers, g is gravity acceleration, ρ is fluid density, and μ is dynamic viscosity of the fluid.

Upon dimensional analysis, the following variables were derived for the normalized scour depth (h_s/D).

$$\frac{h_s}{D} = f\left(\frac{d_{50}}{D}, \sigma_g, \frac{h}{D}, \frac{V}{V_c}, F_r, K_s, \alpha, \frac{L}{D}, \frac{X}{D}\right) \tag{2}$$

where d_{50}/D is sediment coarseness ratio, h/D is flow shallowness ratio, V/V_c is flow intensity, F_r is Froude number, L/D is pier aspect ratio, and X/D is relative clear spacing between the tandem piers.

Local scour around piers is sensitive to the parameters shown in Equation 2. The present research has focused on finding the optimum pier shape to minimize scour depth around isolated and tandem piers, considering the influence of pier shape and alignment. However, h/D, V/V_c, F_r, d_{50}/D, and σ_g are kept constant for all experiments, but K_s, L/D, α, and X/D are varied. The experiments were not influenced by flow shallowness and sediment coarseness [31, 61].

2.2. Pier Models

Three different pier models (M1, M2, and M3) were investigated for their influence on pier shape on the scour process, as shown in Figure 3-a. The cross-section of the pier-1 is circular (M1) with a diameter (D) of 5 cm. The first modified pier (M2) has a semi-circular shape on one-half side and a triangular shape on the other half. The second modified pier (M3) is a variation of M2, incorporating a small groove on the semi-circular nose. A 0.3 cm thick and 0.5

cm protruding metal plate is fixed in this groove to improve streamlining [14]. The protrusion length is 1/10 of the pier diameter (*D*), and a thickness less than the protrusion length was chosen to minimize the projected area. The M2 pier was tested with both the semi-circular side (M2a) and the triangular side (M2b) facing the flow direction. The cross-sectional area of the M2 and M3 pier models is kept equal to that of M1. The pier models were made of polished teak wood and positioned vertically at a distance of 4.75 m from the inlet. This distance ensures a fully developed flow, where the vertical velocity profile remains constant with longitudinal space according to the logarithmic velocity law. Tests with the proposed piers were conducted for eight different skew angles (α = 0°, 5°, 10°, 15°, 20°, 25°, 30°, and 45°). Scour depth measurements were obtained using a 2 mm diameter digital point gauge with an accuracy of ± 0.5 mm.

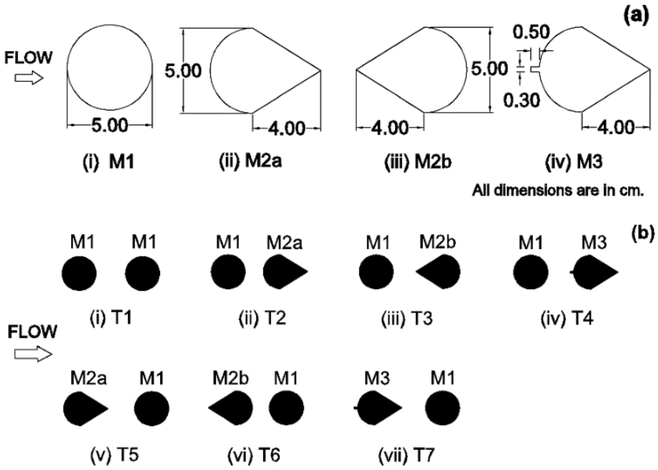

Figure 3. Diagram showing: (a) pier models; and (b) different tandem arrangements

Experiments with the tandem arrangement of piers were conducted by placing the modified-shaped piers in different combinations with the circular pier (Figure 3-b) at different clear spacing (*X*) of 0.5*D*, 1.0*D*, 1.25*D*, 1.5*D*, 1.75*D*, 2.0*D*, and 2.5*D*. In Figure 3b, arrangement T1 consists of two circular piers in tandem. Arrangements T2, T3, and T4 were designed with a circular front pier followed by M2a, M2b, and M3 as rear piers, respectively. T5, T6, and T7 were designed with a circular rear pier and M2a, M2b, and M3 as front piers, respectively. The above arrangements are proposed considering that a circular pier exists, and the modified pier will come up on either side of it. The front pier was placed at a distance of 4.75 m from the inlet, while the rear pier was positioned corresponding to the front pier at the required clear spacing (*X*).

2.3. Flow Conditions

The flow depth (*h*) was maintained at 12 cm so that the flow shallowness ratio (*h/D*) was less than 3 [61], which ensured that the flow depth was enough for scour formation. Based on the Neill [62] approach, the critical velocity for the sand movement is V_c = 0.29 m/s. The flow intensity (V/V_c), the ratio between mean flow velocity (V = 0.26 m/s) and critical velocity (V_c = 0.29 m/s), has been maintained as 0.9 (≤ 1) to ensure sediment movement under clear-water scour conditions [63]. The experiments were conducted at a flow rate (Q) of 0.027 m^3/s. Based on the upstream flow depth (h), the Froude number $\left(F_r = \frac{V}{\sqrt{gh}}\right)$ and Reynolds number $\left(R_e = \frac{\rho V h}{\mu}\right)$ of the flow are calculated as 0.24 and 31200 (which represent sub-critical and turbulent flow conditions), respectively. The densimetric Froude number, $F_{ds} = \frac{V}{\sqrt{g(S-1)d_{50}}}$ = 2.73. All the tests were performed under steady, uniform flow and clear-water scour conditions.

In hydraulic modeling of pier scour, the scale effects are inevitable [64] and depend on the Reynolds number, Froude number, Shields parameter (θ), bed, and pier roughness. In this study, the flume width, pier size, flow depth, and other dimensions were chosen to satisfy the criteria of local scour experiments and minimize the scale effects. Jayaraman [65] stated that the flow (R_e = 31200) and particle ($R_e^* = \frac{\rho u_* d_{50}}{\mu}$ = 8.57) Reynolds numbers should be large enough to minimize viscous and scale effects, respectively. Where, u_* is the shear velocity $= \sqrt{ghS_o}$ = 0.0153 m/s. In addition, the relative roughness (k/h = 0.005) must be less than 0.2 to limit boundary and scale effects on the model, where k is the mean bed surface roughness. In the present study, the θ = 0.026 is less than the threshold limit (= 0.056) for sediment motion [65, 66].

2.4. Experimental Procedure

Before each experiment, the sediment bed was leveled using metal screeds. The initial bed elevations were then measured using the point gauge. Piers were installed vertically at a distance of 4.75 m from the inlet. The bed surrounding each pier was protected with 3 mm thick acrylic sheets to prevent excessive initial erosion. The flow was gradually introduced into the flume to ensure no air bubbles in the voids. After the flow attained the desired discharge and depth by parallel operating the gate valve and tailgate, the flow velocity (V = 0.26 m/s) was calculated using the 3-point averaging method with point velocities at depths of 0.2h, 0.6h, and 0.8h measured from the water surface using the Vectrino Acoustic Doppler Velocimeter (ADV). The measured velocities on various vertical planes along the streamwise direction were subsequently used to establish a logarithmic velocity profile and verify the fully developed flow. The acrylic sheets were withdrawn without disturbing the flow and sediment bed. The flow depth and discharge were monitored consistently to ensure the required flow conditions throughout the test period. Temporal scour depths relative to the initial bed level were measured using the digital point gauge along the pier's periphery at key locations: the pier front, wake, and side flanks. Measurements were taken at 5-minute intervals during the first hour, followed by 30-minute intervals until the scour hole attained an equilibrium state. The frequency of the readings was higher at the initial stage to acquire the high initial scouring rate; after that, it decreased. The flume glass walls were helpful in visually observing the flow structure and scouring around the pier. After completing the experiment (~18 h), the flow was gradually stopped without causing any disturbance to the developed scour hole pattern. The sand bed was drained off using the outlet valve, and the maximum scour depth at the equilibrium state was measured with the point gauge. Photographs of the scour hole were captured using a camera. This procedure was replicated for all experiments. Figure 4 shows the photographs of the flume (Figure 4-a) and the equilibrium scour hole around the conventional circular pier, M1 (Figure 4-b).

Figure 4. Photographs of (a) experimental setup and (b) scour hole around the circular pier (M1)

2.5. M5 Model Tree

A Decision Tree (DT) is a machine-learning algorithm used for classification and prediction tasks. The DT resembles an inverted tree (Figure 5a), where the topmost node is the root node, and the bottommost nodes are the leaves. The Model Tree (MT) is another classification and regression technique that employs a multivariate linear regression model at the leaf nodes and operates based on the principles of the DT algorithm. The MT divides a complex problem into multiple sub-problems, which are combined to obtain the outcome [67]. The M5 model tree (M5) is a popular algorithm among MTs that can generate easily understandable formulas [46]. The M5 involves two phases: creating a DT using linear regression and extracting knowledge from it [67]. In the first phase, linear regression models recursively split data points into subsets. This splitting is guided by the standard deviation (SD) of the subset values, with the goal of minimizing variability by evaluating each parameter at its corresponding node. The SD reduction (SDR) is calculated using the following formula:

$$\mathrm{SDR} = \mathrm{SD}(T) - \sum \frac{|T_i|}{|T|} * \mathrm{SD}(T_i) \tag{3}$$

where T is the set of data records that have reached the node, T_i is the subset of data records that have the i^{th} outcome of the potential test, and SD is standard deviation.

The data in the sub-tree nodes have lower SD values than their parent nodes due to the splitting of the SDR factor. To identify the input parameter that maximizes the reduction in error, each attribute at a node is evaluated, and the anticipated error reduction is computed. However, this iterative process has the potential to create a large tree structure that overfits the data. The process terminates when the SDR reaches less than 5% of the original dataset SD or when only a few instances are left [68]. During the second phase, linear regression models are constructed for each sub-domain using the data associated with the respective leaf. To prevent overfitting, the overgrown tree is pruned when the predicted error of the sub-tree is lower than the expected error. Sub-trees that do not contribute to an improvement in the model's accuracy are pruned, and linear functions are applied to each pruned sub-tree. Following the pruning process, a smoothing procedure is implemented to reduce abrupt discontinuities between neighboring linear models in the leaves, thereby enhancing prediction accuracy [8].

Figure 5 presents a graphical representation of the M5 model tree, employing a basic instance with two input variables, X1 and X2, and an output variable, Y. The M5 algorithm divides the input space $X1 \times X2$ into three linear regression models (LM1 to LM3) at the leaf nodes (Figure 5-a). The model comprises $Y = a(X1) + b(X2) + c$, with regression constants a, b, and c. Figure 5-b displays the relationship among the branches as a tree diagram.

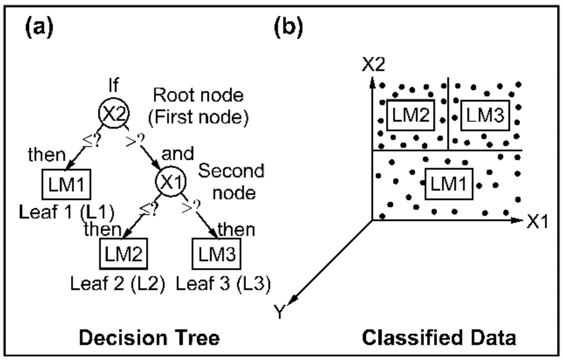

Figure 5. Structure of an M5 model tree

2.6. Performance Evaluation Criteria

The accuracy of the developed M5 models and existing equations is assessed using statistical indices such as coefficient of determination (R^2), root mean square error (RMSE), and discrepancy ratio (DR).

$$R^2 = \left(\frac{n\sum xy - (\sum x)(\sum y)}{\sqrt{[n\sum x^2 - (\sum x)^2][n\sum y^2 - (\sum y)^2]}}\right)^2, 0 \leq R^2 \leq 1 \quad (4)$$

$$\text{RMSE} = \sqrt{\frac{\sum(x-y)^2}{n}} \quad (5)$$

$$\text{DR} = \frac{1}{n}\sum\frac{y}{x} \quad (6)$$

Where x and y in Equations (4-6) are the measured and predicted scour depths, respectively, and n = number of datasets. A well-performing model is determined by lower RMSE, minimal under-predictions (DR $\geq$ 1), and higher R^2 values.

3. Results and Discussion

Three different pier models were investigated to evaluate the influence of pier shape and alignment on local scour, with results presented in terms of maximum scour depth and its temporal variation for both isolated piers and piers in tandem. The test duration (t_e = 18 hours) was chosen to ensure the scour hole reached an equilibrium state, where the rate of scour depth increment fell below 1 mm in 4 hours, as recommended by Ettema [61]. Thus, an asymptotic state in scour depth variation was found between 6 and 12 h. At σ_g of 1.39 (for uniform sediment), armoring occurred at the bottom edge of the scour hole with a mean sediment size of 0.83 mm.

The circular and modified piers were tested thrice (at $\alpha = 0°$) to check the quality of the scour depth measurements, and the measurement error observed was less than 4%. The scour is represented as a normalized scour depth (H^*), calculated as the ratio of the measured scour depth relative to the initial bed level (h_s) and the pier width (D). Similarly, the time scale of scour on the plots is non-dimensionalized (time ratio = T^*) by considering the ratio between scour at a given time (t) and the time to equilibrium scour (t_e). Also, the equilibrium H^* of the piers in tandem is plotted against the clear spacing (X/D) to determine the optimum spacing between the piers. In addition, the M5 models are developed for scour depth prediction at different-shaped isolated and tandem piers using the experimental data from the present study and literature. The accuracy of these M5 models is compared with the existing regression equations.

3.1. Scour Depth around Aligned Piers

The pier's shape significantly influences the local scour, scour hole geometry, and location of maximum scour depth [14]. It was observed that the maximum scour depth was located at the upstream nose for M1, M2a, and M3 piers due to the effect of the downflow and horseshoe vortices [42]. For the M2b pier, the deepest scour depth occurred near the side flanks or center of the pier due to its sharp nose opposite the flow direction, leading to the flow separation near the downstream nose. Keshavarz et al. [22] and Vijayasree et al. [19] also reported similar observations for sharp-nosed piers. The eroded sediment was deposited downstream, where the flow reverted to the approach flow velocity. Figure 6 shows the temporal variation of the normalized scour depth (H^*) for different pier models. These results are compared with the experimental results of Mia and Nago [69] of D = 6 cm, d_{50} = 1.28 mm, F_r = 0.25, and V/V_c = 0.71. For the conventional circular pier M1, the equilibrium H^* was observed as 1.02 and 1.41 in the present study and Mia and Nago [69], respectively. The difference in H^* values might be due to the larger pier size and higher Froude number in the earlier study. However, the measured maximum scour depth for the M1 pier is in close agreement with the empirical equation of Hancu [40], having a maximum H^* equal to 1.07. It was also observed that for M1, equilibrium scour was attained at T^* = 0.6, whereas for M2a, M2b, and M3, it was achieved at T^* = 0.4. This shows that the modified piers reach an equilibrium scour state much earlier than the circular pier. Reducing the scouring rate of modified piers can lower the risk of scour failures during short-duration flood events [5]. Also, the modified piers (M2a, M2b, and M3) reduced scour depth because the flow separation decreased at the pier face; thus, the effect of horseshoe and wake vortices is less compared to the M1 pier. Baranwal et al. [14] also reported similar results on scour depth at sharp-nosed piers. The maximum decrease in the scour depth for M2a, M2b, and M3 piers is 23.5%, 50%, and 55% compared to M1, respectively.

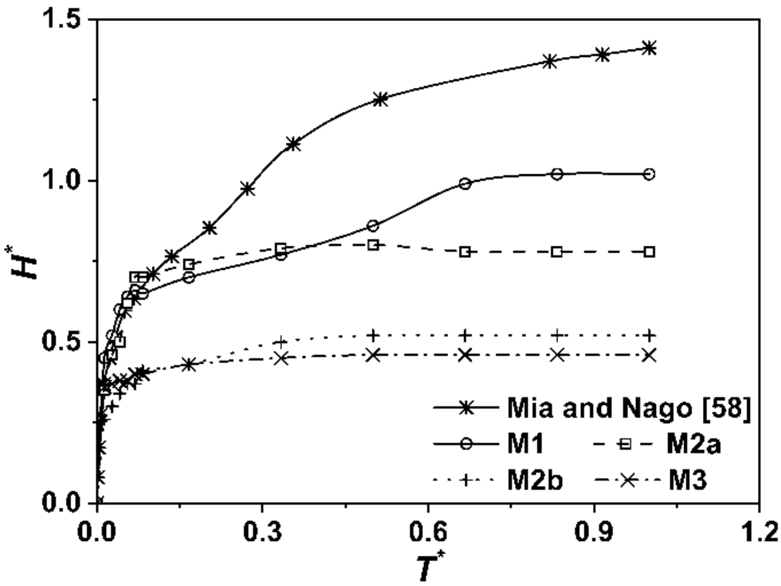

Figure 6. Temporal variation of H^* for isolated piers

The shape factors (K_s) at equilibrium scour are 1.0, 0.765, 0.51, and 0.45 for M1, M2a, M2b, and M3 piers, respectively. These results suggest that these multiplying factors should only be applied when the piers are aligned with the flow. Further, the study confirms that the lowest H^* (= 0.46) was found for M3 due to the inclusion of the metal plate at the pier nose, which caused an instant bifurcation of the approach flow and a shift of the flow separation point towards the downstream side. The performance of M3 is efficient in reducing local scour among all the pier models tested. From the results, it is observed that the use of both M2b and M3 piers could be an effective countermeasure against local scour around bridge piers.

3.2. Effect of Pier Skew Angle

The skew angle (α) at non-circular pier shapes is one of the predominant aspects that decides the performance. This study included α values only up to 45° since skew angles of more than 45° are practically rare [70]. For M2a and M3 piers, the point of deepest scour was located at the leading face when aligned to the flow but the deepest point moved along the exposed face when the piers were skewed. However, the location of maximum scour depth for the M2b pier was found closer to the side flanks while $\alpha \leq 20°$ [20]. Later, it shifted to the front due to increased flow disturbance, which introduced by the presence of pier skewness for $\alpha > 20°$. Further, the rate of scour is greater for higher skew angles ($\alpha > 20°$) due to more projected width, which leads to the change in flow separation point and increased strength of the downflow, horseshoe, and wake vortices [12, 30]. Figure 7 illustrates the scour pattern at the M2a pier with a 45° skewness relative to the flow direction. The scour hole exhibited a notable asymmetry with α = 0° [9, 31].

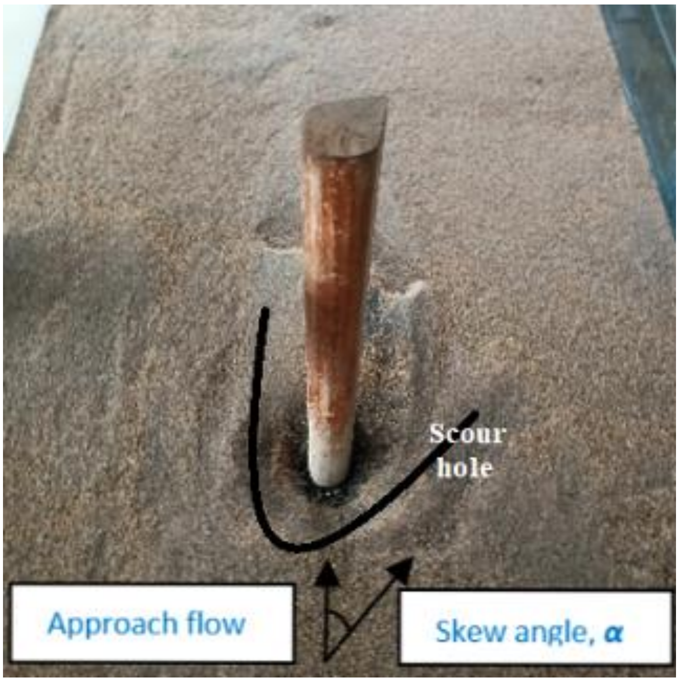

Figure 7. Equilibrium scour hole around M2a pier with α = 45°

Table 1 summarizes the effect of the skew angle (α) on scour depth (H^*) and the corresponding skew factors (K_α). The K_α values were obtained by normalizing the scour depth with scour depth at α = 0°. The scour depth is influenced by the portion of the pier nose exposed to the approaching flow. Lower scour depths were observed for modified piers aligned with the flow. However, higher scour depths were observed for the skewed piers due to greater disturbance of the flow. This observation agrees with the earlier findings related to skewed rectangular piers [36]. It can be inferred from these findings that the scour depth is directly proportional to the skewness of a non-circular pier [38]. Pier shape

Table 1. Effect of pier skewness on scour around the modified-shaped piers for various skew angles (α)

Skew angle (α)	Normalized max. scour depth, H^* (= h_s/D)			Skew factor (K_α)		
	Pier shape					
	M2a	M2b	M3	M2a	M2b	M3
0°	0.78	0.52	0.46	1	1	1
5°	0.88	0.52	0.54	1.13	1	1.17
10°	0.9	0.54	0.59	1.15	1.04	1.28
15°	0.92	0.56	0.62	1.18	1.08	1.36
20°	0.94	0.62	0.64	1.20	1.19	1.39
25°	0.96	0.64	0.66	1.23	1.23	1.43
30°	1.0	0.68	0.7	1.28	1.31	1.52
45°	1.02	0.84	0.82	1.31	1.61	1.78

In Figure 8, the K_α versus skew angles (α) of the M2 and M3 piers are compared with the Laursen & Toch [20] design curves for the skewed rectangular pier (pier aspect ratio, L/D = 2 and 4). For each skew angle α, the flow field and scour mechanism at the skewed piers are distinct [26, 29]. It can be observed from Figure 8 that the K_α changes non-linearly with α, with an indefinite pattern of variation for M2 and M3 piers. The scour depth is highly sensitive to the skew angle (α > 5°) [31, 32, 34]; the scour depth around M2a and M3 piers increased by 13% and 17.5%, respectively. An alteration in the flow pattern, boundary layer separation, and strength of wake vortices, enhanced flow turbulence [29], and their asymmetrical geometry may have contributed to this increase [71]. However, for the M2b pier, changes in skew angle up to 5° do not impact the scour depth because the sharp nose induces immediate flow bifurcation, aligning with observations by Moussa [72].

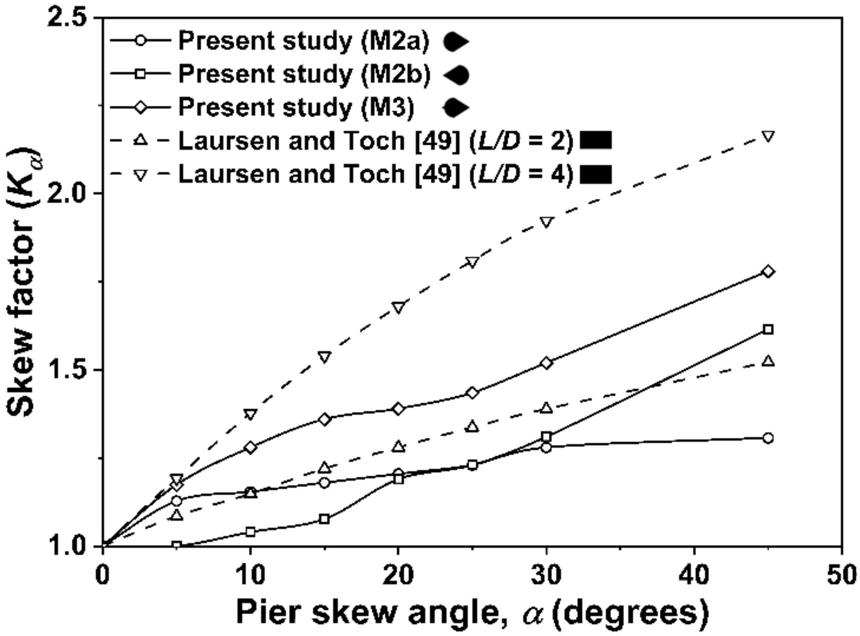

Figure 8. Skew factor, K_α vs. pier skew angle, α

Furthermore, Figure 8 reveals a minor deviation in K_α values between the modified piers and the rectangular pier with *L/D* = 2. However, when comparing the *L/D* = 4 trends, there is a significant deviation in the K_α curves, implying that the pier aspect ratio (*L/D*) substantially affects the K_α values. Additionally, the sensitivity of K_α to the skew angle is much higher for rectangular piers than for the modified piers used in the study.

The effectiveness of streamlining on reducing scouring was diminished when the piers were made more skewed, especially at the M2a and M3 piers. These modified pier shapes became blunt-nosed at higher skew angles. However, the impact was less at the M2b pier because the flow interacted less with it due to a decreased pressure field. These findings suggest that piers with a sharp, streamlined shape are better at reducing the scour depth. A symmetrical scour hole emerges when the modified piers are aligned with the flow. However, changes in the flow structure and hydrodynamics around the skewed piers cause alterations in the geometry of the scour hole and sediment ridge morphology [72].

3.3. Piers in Tandem Arrangement

Experiments were conducted to analyze the effect of pier shape and spacing between tandem piers on local scour. For this purpose, the circular pier (M1) and the modified pier models are placed in various tandem arrangements with longitudinal clear spacing (*X*) ranging from 0.5*D* to 2.5*D*. The clear spacing is considered up to 2.5*D* since the sheltering effect diminishes when *X/D* exceeds 3, according to Liang et al. [73]. Figure 3b displays different tandem arrangements that were studied. The results regarding the maximum scour depth ratio (H^*) for both piers in tandem are presented.

Figure 9 shows the variation in maximum scour depth (H^*) for different clear spacing (*X/D*) between tandem circular piers (T1). Experiments were conducted using three different sediments for this purpose (d_{50} of 0.19 mm, 0.32 mm, and 0.56 mm). The location of the maximum scour depth was in front of the upstream pier, as reported by Wang et al. [74]. The measured H^* values for the isolated circular pier are 1.47, 1.42, and 1.02 for d_{50} = 0.19 mm, 0.32 mm, and 0.56 mm, respectively. It can be observed that the scour depth decreases with an increase in sediment size. The front pier experienced more scour depth than the rear pier [36]. Compared to an isolated pier (M1), the rear pier had a reduced scour depth due to the sheltering effect, upflow behind the front pier, and sediment deposition or live-bed conditions at the rear pier [48, 51, 53, 54, 57].

From Figure 9, we observe that for d_{50} = 0.19 mm, the scour depth gradually increases up to a critical spacing of 1.2*D*, and after that, it decreases with an increase in clear spacing for both front and rear piers. However, for d_{50} = 0.32 mm, the front pier scour depth decreases up to the critical spacing of 1.2*D* and increases afterward, but the rear pier scour depth decreases with a further increasing spacing. Whereas, for d_{50} = 0.56 mm, the scour depth decreased till the critical spacing of 1.75*D* and increased thereafter. Khaple et al. [53] also made similar results for the tandem circular piers. For both d_{50} = 0.32 mm and 0.56 mm, the scour phenomenon is identical for the front and rear piers, although the rear pier scour depth slightly increased at 2*D* for d_{50} = 0.56 mm. At the critical spacing, the H^* values for the front and rear pier are observed as 1.61 and 1.47, 1.18 and 0.94, and 0.51 and 0.44, for d_{50} = 0.19 mm, 0.32 mm, and 0.56 mm, respectively. It can be inferred that the critical spacing between the piers increases with increased sediment size. For the front pier, the scour depth is inversely proportional to the sediment size up to the critical spacing for d_{50} > 0.19 mm. In the tandem arrangement, for d_{50} = 0.32 mm and 0.56 mm, the H^* of the front pier is less than that of an isolated pier, but for d_{50} = 0.19 mm, it is more. Khaple et al. [49] performed clear-water experiments (d_{50} = 0.95 mm) with circular piers (D = 4 cm and 7.7 cm) that were placed in a tandem arrangement at various clear spacing (X = 4D to 16D). It was reported that the scour depth at the front pier was independent of spacing between the piers. This suggests that the interference effect between the piers in tandem is present till $X \leq 2.5D$, and there is no effect beyond $X \geq 4D$. Here, the wake region of the front pier is suppressed by the horseshoe vortex formed upstream of the rear pier.

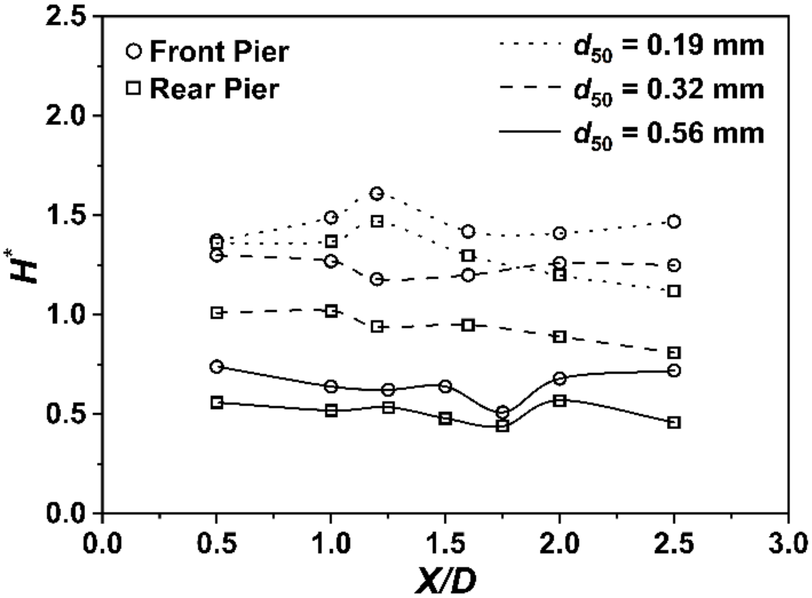

Figure 9. Variation of H^* for different X/D in the tandem arrangement of circular piers

Table 2 presents the variation in H^* values for different tandem pier arrangements (d_{50} = 0.56 mm) and spacing. Where the H_f^* and H_r^* are the non-dimensional scour depths for the front and rear piers, respectively. The location of maximum scour depth varied across these tandem arrangements. The scour depth for both the front and rear piers was reduced for all combinations with modified piers (Table 2) compared to circular piers at the critical spacing of 1.75D, except M2b placed at the upstream side of the circular pier. It is due to the pier shape effect and interference of wake vortices of the front pier and the horseshoe vortex of the rear pier. The H_f^* is reduced by 31.37%, 29.41%, and 17.65% compared to the T1 arrangement by replacing the downstream circular pier with M2a, M2b, and M3 (T2, T3, and T4), at clear spacings (X) of 1.0D, 1.5D, and 1.25D, respectively. These results suggest that if a new bridge is to be constructed downstream of an existing bridge with a circular pier, M2a at X = 1.0D is preferable. Similarly, the maximum scour depth reduction for a circular rear pier (H_r^*) was 22.7%, 20.45%, and 22.73% by placing M2a, M2b, and M3 as the front pier (T5, T6, and T7) at a clear spacing (X) of 1.75D, 0.5D, and 1.75D, respectively. It shows that a circular pier can be replaced by an M3 pier at the upstream side of an existing circular pier at a spacing of 1.75D to reduce the scour depth. Earlier, it was discussed that the M3 pier scour depth was minimal compared to other pier models. Similarly, the combination with an M3 pier placed upstream or downstream of a circular pier exhibits the least scour depth for both the piers (T4 and T7) at any spacing X. Figure 10 shows the equilibrium scour hole around tandem piers of T7 arrangement spaced at X/D = 1.25. At this spacing, the scour holes of both the M3 and M1 piers were combined.

Table 2. Front and rear piers scour depth for different tandem arrangements

Tandem arrangement	X/D = 0.5		X/D = 1.0		X/D = 1.25		X/D = 1.5		X/D = 1.75		X/D = 2.0		X/D = 2.5	
	H_f^*	H_r^*	H_f^*	H_r^*	H_f^*	H_r^*	H_f^*	H_r^*	H_f^*	H_r^*	H_f^*	H_r^*	H_f^*	H_r^*
T1	0.74	0.56	0.64	0.52	0.62	0.54	0.64	0.48	0.51	0.44	0.68	0.57	0.72	0.46
T2	0.58	0.36	0.35	0.29	0.5	0.43	0.47	0.44	0.42	0.37	0.49	0.36	0.37	0.33
T3	0.42	0.25	0.42	0.34	0.46	0.35	0.36	0.17	0.46	0.3	0.41	0.19	0.5	0.26
T4	0.53	0.33	0.52	0.44	0.42	0.37	0.55	0.55	0.47	0.51	0.47	0.39	0.47	0.34
T5	0.48	0.44	0.48	0.40	0.35	0.37	0.39	0.36	0.45	0.34	0.39	0.37	0.38	0.34
T6	0.4	0.35	0.6	0.4	0.57	0.5	0.46	0.48	0.36	0.5	0.34	0.43	0.45	0.46
T7	0.34	0.35	0.32	0.4	0.30	0.38	0.32	0.40	0.29	0.34	0.34	0.35	0.31	0.38

Figure 10. Scour hole around M3 and M1 piers placed in tandem arrangement (T7) at *X/D* = 1.25

In addition, the modified piers can be used as an effective scour countermeasure if a new bridge is proposed to be built adjacent to an existing bridge with circular piers. In this scenario, the experimental results with piers in tandem arrangement are useful in bridge planning.

3.4. Scour Depth Prediction using M5 Models

Scour depth prediction is crucial for designing pier foundations. In this study, individual M5 models were developed to predict the maximum scour depth (h_s/D) around isolated and tandem piers. An improved version of the M5 algorithm (M5') available in an open-sourced WEKA software was used to develop these M5 models [75]. The training and testing of each M5 model took less than a minute. Initially, the dataset was imported into the WEKA software, and the classifier M5P was selected. Later, the number of instances in each leaf present in the M5 model was determined. Different combinations of input parameters (Equation 2) were tested in developing these models, and the most accurate one was identified based on higher R^2 and lower RMSE values. The developed models were validated using a testing dataset, and a sensitivity analysis was conducted to assess the significance of each input parameter on scour depth prediction.

3.4.1. Isolated Pier

The data from the present experimental study and the literature [7, 9, 14, 19, 21, 29, 76, 77] are used to develop the M5 model. These datasets pertain to scour around different-shaped piers in cohesionless soils under clear-water scour conditions. The data was normalized [68] through dimensional analysis (Equation 7).

Non-dimensional maximum scour depth, $\frac{h_s}{D} = f\left(\frac{d_{50}}{D}\ \frac{h}{D}\ \frac{V}{V_c}\ K_s\ \frac{L}{D}\ \frac{\alpha}{45}\right)$ (7)

where L/D is the pier aspect ratio, α is the skew angle in degrees, and K_s is the pier shape factor with K_s = 1, 1.11, 1, 0.9, 0.86, 0.85, 0.88, 0.55, 1.01, 0.6, 0.75, 0.9, and 0.73 for circular, rectangular, round-nosed, sharp-nosed, octagonal, oblong, joukowsky, streamlined, chamfered, hexagonal, elliptical, rhombus, and lenticular, respectively [9, 20, 27, 31, 32, 33, 61, 78]. Bhattacharya et al. [79] and Kumar et al. [45] procedure was followed to divide the dataset randomly (207 data points) for training (75%; 156 data points) and testing (25%; 51 data points) of the M5 model. Thus, the data range considered for the training and testing (Table 3) is approximately similar. The developed M5 model tree for predicting scour depth (h_s/D) around isolated piers employing nine rules is shown in Figure 11.

Table 3. Non-dimensional parameters data used for isolated pier

Variable	Training data				Testing data			
	Min.	Max.	Mean	SD	Min.	Max.	Mean	SD
d_{50}/D	0.004	0.027	0.013	0.007	0.004	0.027	0.014	0.007
h/D	1	5.5	2.974	0.958	1.333	5.5	3.245	1.025
V/V_c	0.309	0.96	0.757	0.192	0.359	0.96	0.753	0.201
K_s	0.45	1.11	0.882	0.183	0.45	1.11	0.888	0.188
L/D	1	10	3.381	2.163	1	10	3.515	2.119
$\alpha/45$	0	1	0.147	0.303	0	1	0.111	0.261
h_s/D	0	6.05	1.449	0.987	0	6.94	1.648	1.34

Note: Min.: Minimum; Max.: Maximum; and SD: Standard deviation.

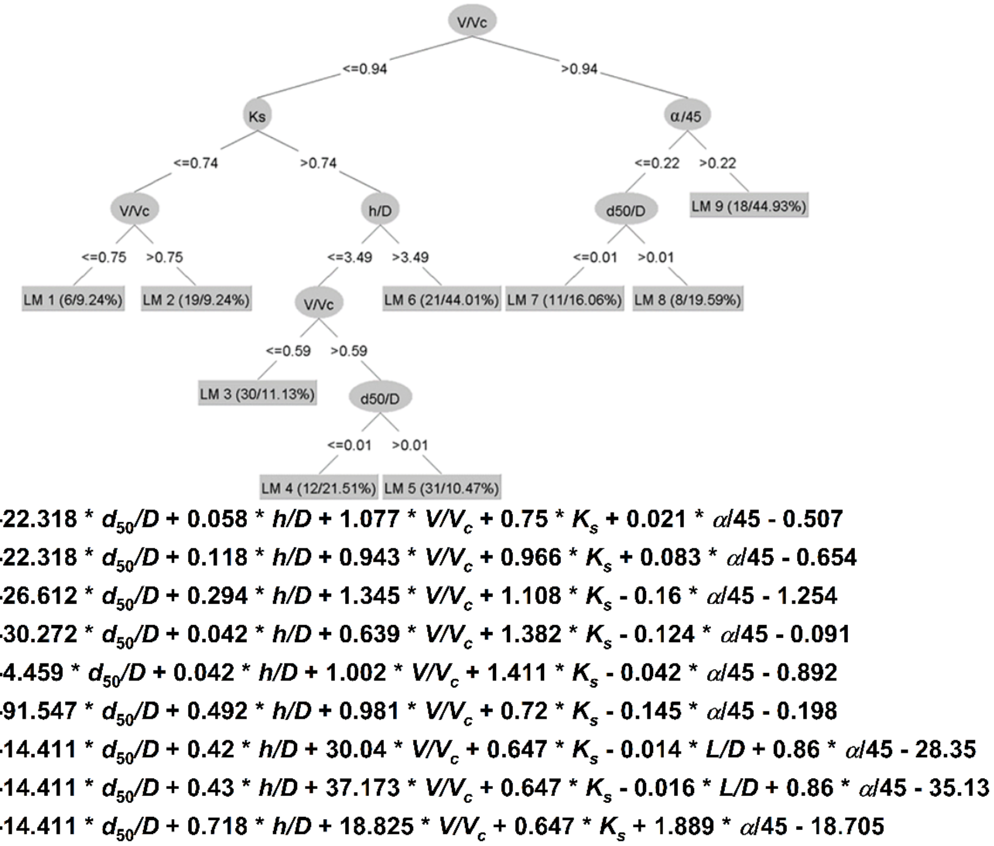

Figure 11. M5 model for predicting scour depth (h_s/D) around isolated piers

The performance of the model, both in training and testing, is shown in Figures 12-a and 12-b, respectively. In the training phase, the model has R^2 = 0.894, RMSE = 0.332, and DR = 1.082. These high R^2 and low RMSE values indicate a strong correlation between the h_s/D and input variables. Although, a minor variation between the training (Min. = 0, Max. = 6.05, Mean = 1.449, SD = 0.987) and testing (Min. = 0, Max. = 6.94, Mean = 1.648, SD = 1.34) data as seen in Table 3, the M5 model could be able to predict the scour depth accurately (R^2 = 0.837, RMSE = 0.625, and DR = 1.018). In Figure 12-a, the model is under-predicting the scour depth for a few data points of Al-Shukur and Obeid [7], Fael et al. [9], and Farooq & Ghumman [21]. The model is over-predicting the scour depth for rectangular piers with α = 0 - 5° (Ahmad et al. [29]), aligned chamfered, sharp-nosed, and lenticular piers (Vijayasree et al. [19]), and modified-shaped piers in the present study with α = 0 - 10°. Thus, it can be inferred that the model is not performing well for skew angles less than 10°. A similar phenomenon is observed during testing (Figure 12-b), that few data points of Al-Shukur and Obeid [7], Fael et al. [9], and Farooq & Ghumman [21]; and Ahmad et al. [29], Vijayasree et al. [19], and the present study are under-predicting and over-predicting, respectively. However, in Figure 12-b, about 60% of the predictions during testing of the M5 model fall within an error of ± 20%, signifying the model's ability to predict the h_s/D accurately. The model predictions for the proposed modified-shaped piers match the experimental results well.

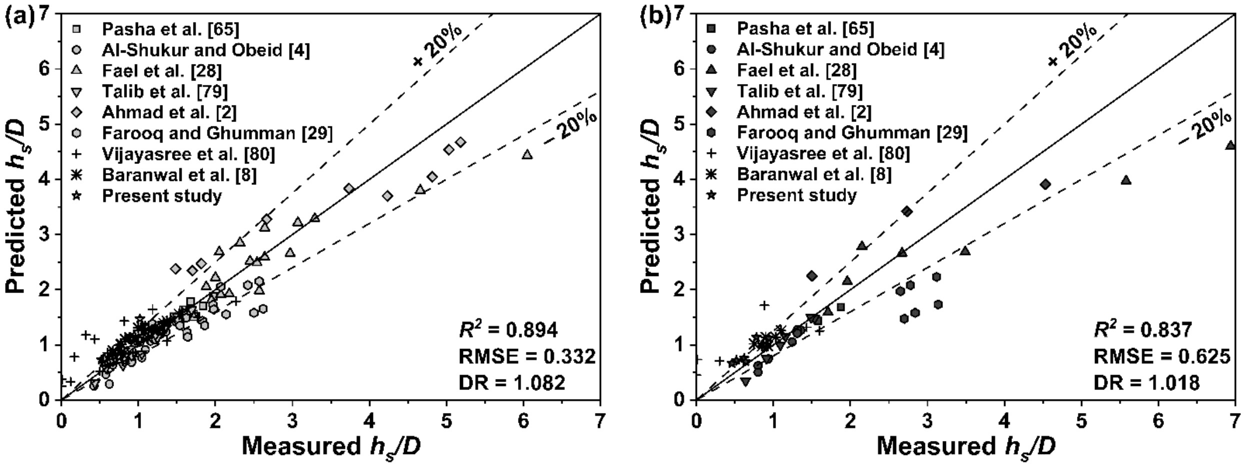

Figure 12. Scatter plots of measured vs. predicted scour depths (h_s/D) during: (a) training; and (b) testing

A sensitivity analysis is performed to identify the most influential parameters for predicting h_s/D. The M5 model was trained multiple times by excluding one of the input variables each time and validated. The testing results are discussed here. From this analysis, it is observed that the skew angle ($\alpha/45$) has significant impact (R^2 = 0.483, RMSE = 0.992) on predicting h_s/D, followed by h/D, K_s, V/V_c, d_{50}/D, and the pier aspect ratio (L/D) has less impact (R^2 = 0.836, RMSE = 0.626), because L/D has interdependency with α and K_s. These results indicate that the proposed M5 model can accurately predict the scour depth using the parameters D, d_{50}, h, V, V_c, K_s, L, and α. However, the accuracy relies not only on the M5 model configuration but also on the input parameters and data quality.

The predicted scour depths from the M5 model are compared with the existing regression-based equations (Figure 13) such as Breusers et al. [42], Melville and Sutherland [31], CSU (Richardson & Davis [32]), Richardson and Panchang [44], and Heza et al. [43]; that have been available for estimating scour depth at different-shaped piers that are aligned and skewed. The predictions of the CSU [32] and Heza et al. [43] equations are more accurate and conservative (DR ≥ 1) than the other equations since these two equations have the Froude number (F_r) as an influential variable. Qi et al. [11] reported similar findings on existing scour equations. In Figure 13, a few data points of Fael et al. [9], Farooq & Ghumman [21], Vijayasree et al. [19], and the present study are far from the best-fit line. Although Vijayasree et al. [19] reported no scour depth for lenticular and chamfered piers, the tested equations showed the presence of scour depth. Whereas, the M5 model performance is good (R^2 = 0.837, RMSE = 0.625). This can be due to the wider range of datasets used and the ability of the M5 model to characterize the non-linear and complex relationship between the parameters.

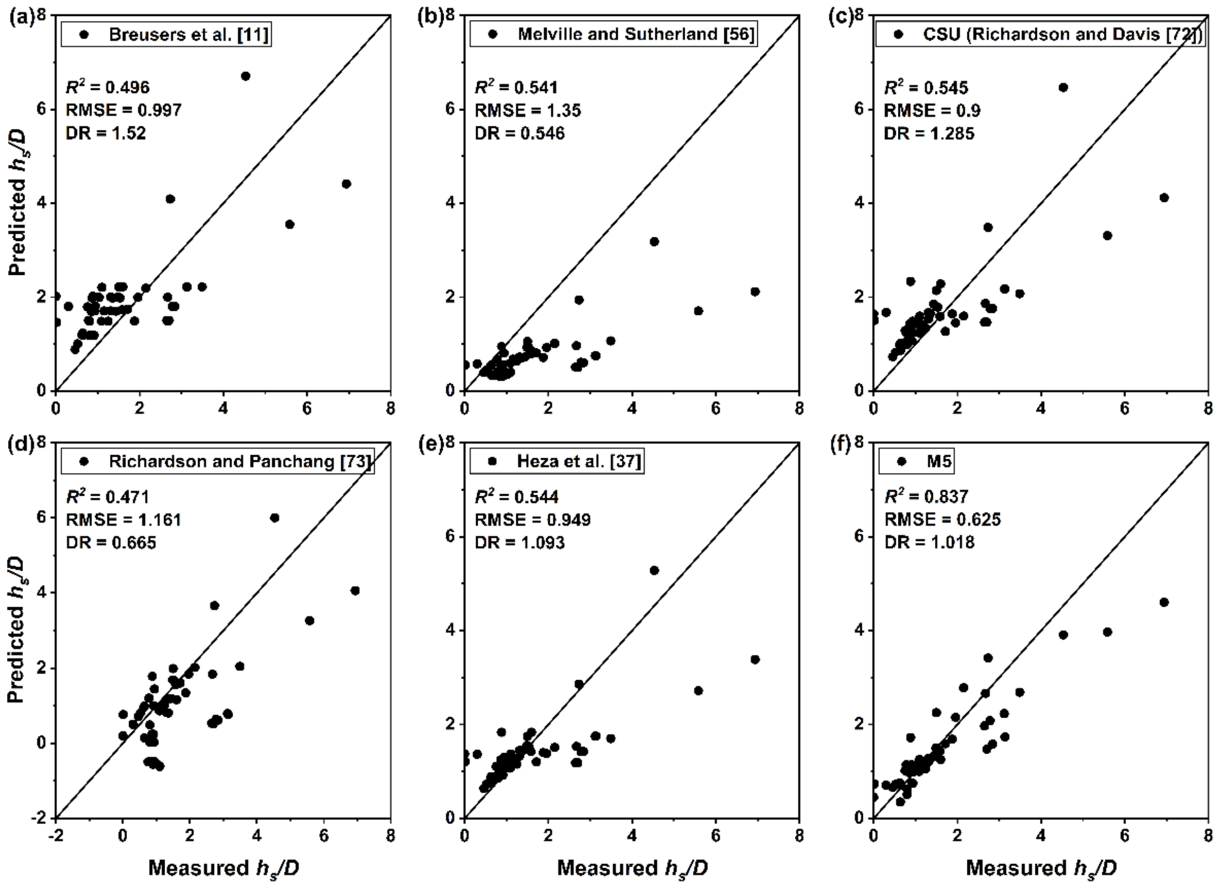

Figure 13. Comparison of M5 model results with regression equations using the testing dataset

The box plot (Figure 14) shows the distribution of residual errors on h_s/D prediction, used to assess the reliability of the M5 model and existing regression equations. It illustrates the residuals at different quartiles (Q25%, Q75%, and IQR), and the whisker distance is the range between the maximum of both positive and negative errors. It can be observed that the CSU [32] and Heza et al. [43] equations are more reliable compared to the other equations. The equations of Melville and Sutherland [31] and Richardson & Panchang [44] are under-predicting h_s/D (DR << 1), endangering bridge safety. Meanwhile, the Breusers et al. [42] equation over-predicting h_s/D (DR >> 1) leads to an uneconomical bridge design. The M5 model, with a smaller box and whisker distance, is relatively more accurate than the existing regression equations. However, both the M5 model and equations have outliers for Fael et al. [9] and Farooq and Ghumman [21] data toward positive residual (or under-prediction). Based on these observations, this study suggests that the M5 model is a viable alternative to the regression equations.

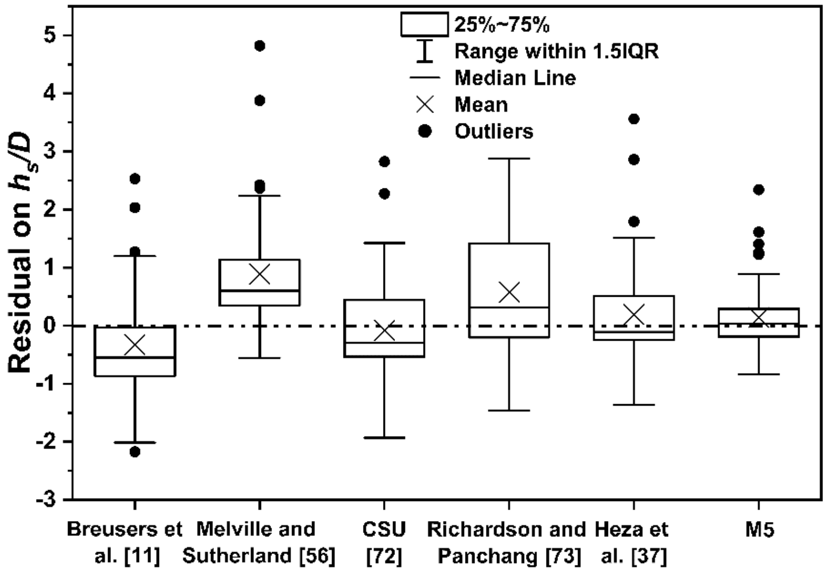

Figure 14. Box plot for residual errors on h_s/D prediction using the testing dataset

3.4.2. Tandem Piers

The experimental data from the present study and the literature data [49, 53, 74, 80-84] were used to develop the M5 models. Among them, Malik & Setia [83] and the present study have the scour data of different-shaped piers (circular, rectangular, and modified-shaped piers) in addition to the circular piers in tandem. The collected data is normalized through dimensional analysis (Equation 8).

$$\text{Non-dimensional maximum scour depth, } \frac{h_{si}}{D} = f\left(\frac{d_{50}}{D}\ \frac{h}{D}\ \frac{V}{V_c}\ \frac{X}{D}\ (K_s)_i\right) \tag{8}$$

where the subscript i refers to a tandem pier position, i.e., front (f) and rear (r). The scour depth of the tandem piers is denoted as h_{sf}/D and h_{sr}/D for the front and rear piers, respectively. Similarly, $(K_s)_f$ and $(K_s)_r$ are the shape factors of the front and rear piers, respectively.

Separate M5 models were developed for the scour depth around front (h_{sf}/D) and rear (h_{sr}/D) piers. Bhattacharya et al. [49] and Kumar et al. [45] procedure followed to divide the collected data (300 data points) for training (75%; 225 data points) and testing (25%; 75 data points) of the M5 models. Table 4 provides the statistical summary of the variables. The developed M5 model tree for scour depth at the front (h_{sf}/D) (employing 12 rules) and rear (h_{sr}/D) (employing 13 rules) piers is shown in Figures 15-a and 15-b, respectively

Table 4. Non-dimensional parameters data used for piers in tandem arrangement

Variable	Training data				Testing data			
	Min.	Max.	Mean	SD	Min.	Max.	Mean	SD
d_{50}/D	0.004	0.035	0.016	0.01	0.004	0.035	0.016	0.01
h/D	1.951	5	2.62	0.702	1.951	5	2.593	0.656
V/V_c	0.449	1	0.861	0.151	0.471	1	0.86	0.135
X/D	0	25	5.506	4.605	0.5	15	5.039	4.269
$(K_s)_f$	0.45	1	0.972	0.112	0.45	1	0.966	0.122
$(K_s)_r$	0.45	1.1	0.972	0.119	0.45	1.1	0.976	0.108
h_{sf}/D	0	2.523	1.206	0.691	0.033	2.458	1.194	0.699
h_{sr}/D	0.033	2.11	1.012	0.577	0.033	2.001	0.999	0.569

Note: Min.: Minimum; Max.: Maximum; and SD: Standard deviation

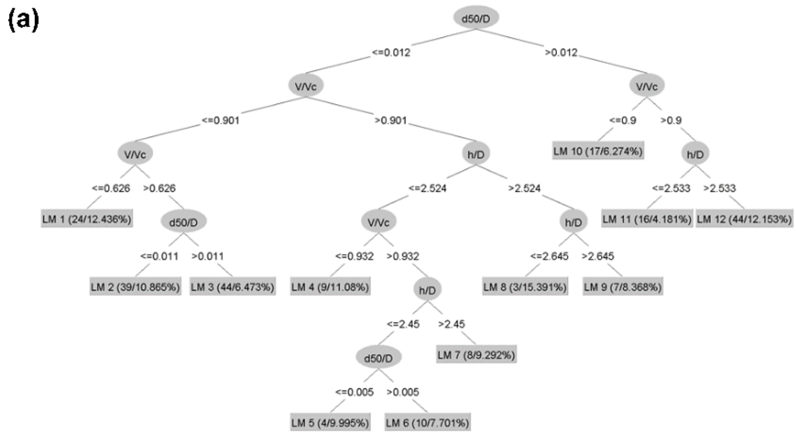

LM 1: $h_{sf}/D = 38.071 * d_{50}/D + 0.069 * h/D + 2.523 * V/V_c + 0.002 * X/D + 0.740 * (K_s)_f + 0.643 * (K_s)_r - 3.085$

LM 2: $h_{sf}/D = -26.989 * d_{50}/D + 0.071 * h/D + 0.986 * V/V_c + 0.003 * X/D + 0.923 * (K_s)_f + 0.751 * (K_s)_r - 1.616$

LM 3: $h_{sf}/D = 33.985 * d_{50}/D + 0.134 * h/D + 2.468 * V/V_c + 0.001 * X/D + 0.696 * (K_s)_f + 0.601 * (K_s)_r - 3.037$

LM 4: $h_{sf}/D = 10.144 * d_{50}/D + 0.001 * h/D + 0.644 * V/V_c + 0.506 * (K_s)_f + 0.43 * (K_s)_r - 0.347$

LM 5: $h_{sf}/D = 8.935 * d_{50}/D + 0.015 * h/D + 0.607 * V/V_c + 0.001 * X/D + 0.506 * (K_s)_f + 0.43 * (K_s)_r - 0.320$

LM 6: $h_{sf}/D = 10.282 * d_{50}/D + 0.015 * h/D + 0.607 * V/V_c + 0.001 * X/D + 0.506 * (K_s)_f + 0.43 * (K_s)_r - 0.338$

LM 7: $h_{sf}/D = 8.935 * d_{50}/D + 0.023 * h/D + 0.577 * V/V_c + 0.002 * X/D + 0.506 * (K_s)_f + 0.43 * (K_s)_r - 0.299$

LM 8: $h_{sf}/D = 9.75 * d_{50}/D - 0.589 * h/D + 0.644 * V/V_c - 0.011 * X/D + 0.506 * (K_s)_f + 0.43 * (K_s)_r + 1.215$

LM 9: $h_{sf}/D = 9.75 * d_{50}/D - 0.176 * h/D + 0.644 * V/V_c - 0.018 * X/D + 0.506 * (K_s)_f + 0.43 * (K_s)_r + 0.078$

LM 10: $h_{sf}/D = 24.907 * d_{50}/D - 0.028 * h/D + 4.647 * V/V_c + 0.287 * (K_s)_f + 0.25 * (K_s)_r - 3.409$

LM 11: $h_{sf}/D = 5.443 * d_{50}/D + 0.086 * h/D + 1.086 * V/V_c - 0.004 * X/D + 0.287 * (K_s)_f + 0.250 * (K_s)_r + 0.032$

LM 12: $h_{sf}/D = 5.443 * d_{50}/D + 0.122 * h/D + 1.086 * V/V_c - 0.006 * X/D + 0.287 * (K_s)_f + 0.25 * (K_s)_r + 0.065$

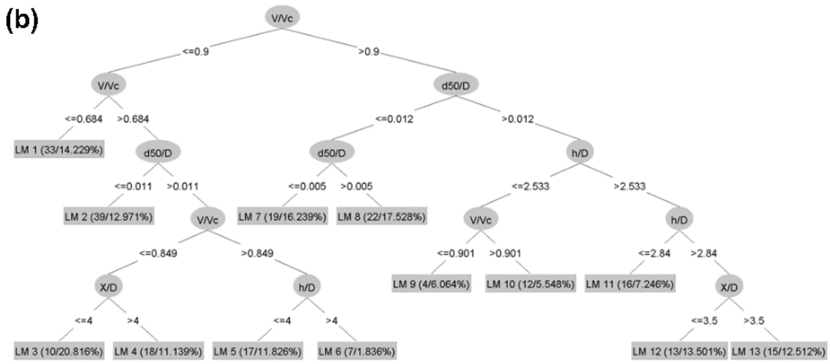

LM 1: $h_{sr}/D = 9.987 * d_{50}/D + 2.086 * V/V_c + 0.005 * X/D + 0.382 * (K_s)_f + 0.43 * (K_s)_r - 1.855$

LM 2: $h_{sr}/D = -50.557 * d_{50}/D + 0.008 * h/D + 0.706 * V/V_c + 0.008 * X/D + 0.464 * (K_s)_f + 0.589 * (K_s)_r - 0.532$

LM 3: $h_{sr}/D = 16.419 * d_{50}/D + 0.063 * h/D + 1.396 * V/V_c - 0.009 * X/D + 0.365 * (K_s)_f + 0.417 * (K_s)_r - 1.555$

LM 4: $h_{sr}/D = 16.419 * d_{50}/D + 0.016 * h/D + 1.599 * V/V_c + 0.021 * X/D + 0.365 * (K_s)_f + 0.417 * (K_s)_r - 1.661$

LM 5: $h_{sr}/D = 31.314 * d_{50}/D - 0.028 * h/D + 1.148 * V/V_c + 0.017 * X/D + 0.365 * (K_s)_f + 0.417 * (K_s)_r - 1.283$

LM 6: $h_{sr}/D = 26.888 * d_{50}/D - 0.036 * h/D + 1.148 * V/V_c + 0.015 * X/D + 0.365 * (K_s)_f + 0.417 * (K_s)_r - 1.168$

LM 7: $h_{sr}/D = 689.556 * d_{50}/D + 0.234 * h/D + 0.155 * V/V_c + 0.176 * (K_s)_f + 0.196 * (K_s)_r - 2.509$

LM 8: $h_{sr}/D = 21.242 * d_{50}/D + 0.101 * h/D + 0.155 * V/V_c + 0.176 * (K_s)_f + 0.196 * (K_s)_r + 0.175$

LM 9: $h_{sr}/D = 3.446 * d_{50}/D + 0.096 * h/D + 0.745 * V/V_c - 0.003 * X/D + 0.176 * (K_s)_f + 0.196 * (K_s)_r + 0.23$

LM 10: $h_{sr}/D = 2.979 * d_{50}/D + 0.096 * h/D + 0.745 * V/V_c - 0.006 * X/D + 0.176 * (K_s)_f + 0.196 * (K_s)_r + 0.245$

LM 11: $h_{sr}/D = 4.713 * d_{50}/D + 0.099 * h/D + 0.476 * V/V_c - 0.004 * X/D + 0.176 * (K_s)_f + 0.196 * (K_s)_r + 0.53$

LM 12: $h_{sr}/D = 5.299 * d_{50}/D + 0.124 * h/D + 1.067 * V/V_c - 0.005 * X/D + 0.176 * (K_s)_f + 0.196 * (K_s)_r - 0.092$

LM 13: $h_{sr}/D = -4.929 * d_{50}/D + 0.121 * h/D + 1.027 * V/V_c - 0.008 * X/D + 0.176 * (K_s)_f + 0.196 * (K_s)_r + 0.3$

Figure 15. M5 models for predicting scour depth (h_s/D) around tandem piers: (a) front pier (h_{sf}/D); and (b) rear pier (h_{sr}/D)

The performance of the M5 model for the front pier scour depth (h_{sf}/D) during training and testing is shown in Figures 16-a and 16-b, respectively. During training, the model has R^2 = 0.965, RMSE = 0.129, and DR = 1.125. A good correlation is observed between the measured and predicted h_{sf}/D. Similarly, the performance of the M5 model in predicting rear pier scour depth (h_{sr}/D) during training and testing is shown in Figures 17-a and 17-b, respectively. In both training and testing, the predicted h_{sr}/D agrees well with the measured values, and the R^2 = 0.967, RMSE = 0.106, DR = 1.083 and R^2 = 0.953, RMSE = 0.123, DR = 1.102, respectively. The M5 model is over-predicting h_{sf}/D for Wang et al. [74] data and non-circular tandem piers data of Malik & Setia [83] and the present study. About 75% of the predictions fall within ± 15% error.

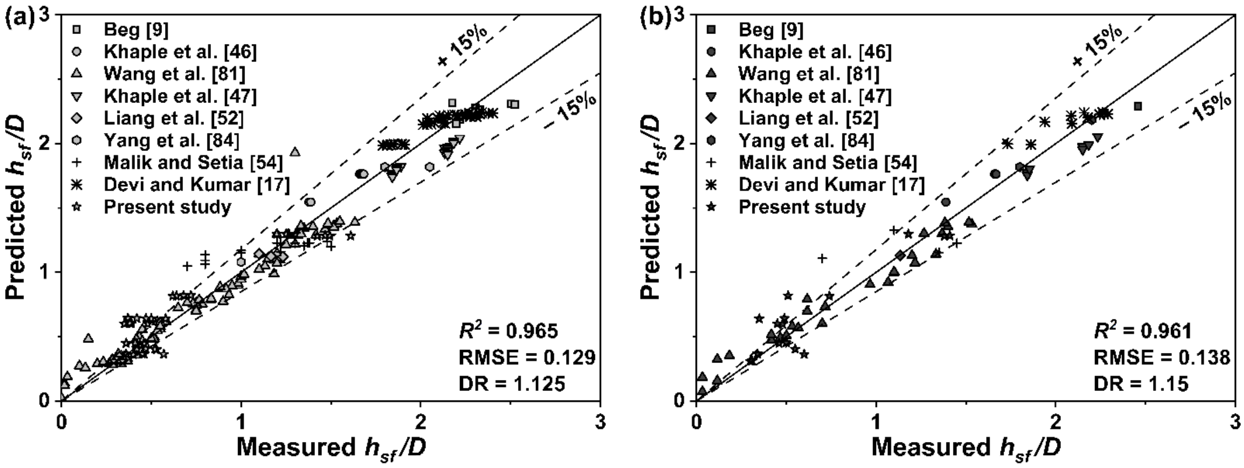

Figure 16. Scatter plots of measured vs. predicted scour depths at the front pier (h_{sf}/D) during: (a) training; (b) testing

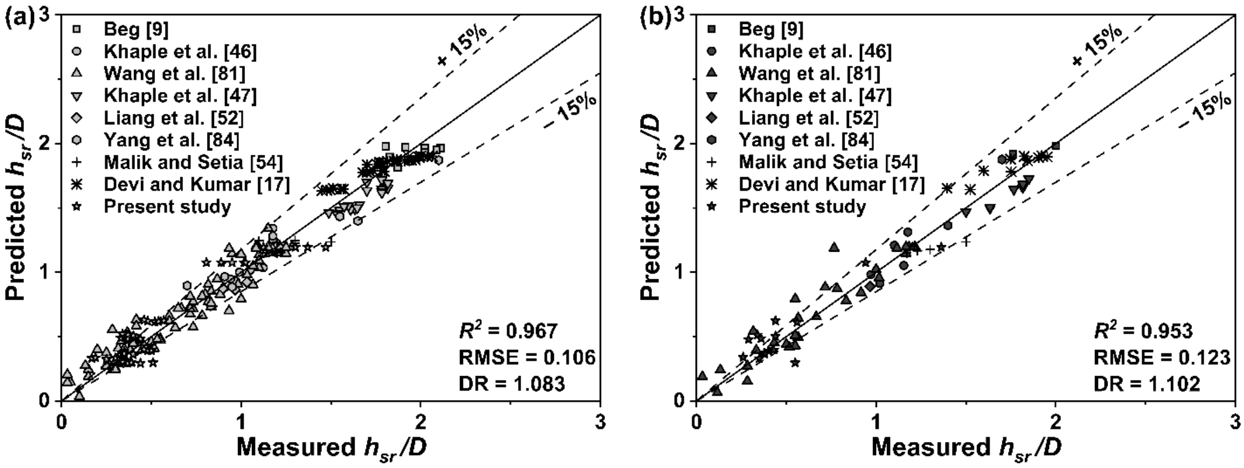

Figure 17. Scatter plots of measured vs. predicted scour depths at the rear pier (h_{sr}/D) during: (a) training; (b) testing

From the sensitivity analysis, it is found that the influence of flow intensity (V/V_c) is more on h_{sf}/D prediction (R^2 = 0.769, RMSE = 0.334) compared to d_{50}/D, $(K_s)_f$, h/D, $(K_s)_r$, and the clear spacing (X/D) has less impact (R^2 = 0.962, RMSE = 0.137). For h_{sr}/D prediction, the flow intensity (V/V_c) has the greatest impact (R^2 = 0.79, RMSE = 0.259), followed by d_{50}/D, X/D, h/D, $(K_s)_f$, and the shape factor of the rear pier $(K_s)_r$ has least impact (R^2 = 0.95, RMSE = 0.126). These results indicate that the M5 model can be used to predict the scour depth of the tandem piers.

4. Conclusion

The experimental study's key finding is an alternate pier shape that reduces local scour. In this study, the isolated piers were tested both aligned and skewed to the approach flow, but the piers placed in the tandem arrangement were tested without skewness. The clear-water experimental results indicated that the pier shape and alignment significantly affect scour rate and depth. The maximum scour depth was reduced by up to 55% for the modified-shaped pier models compared to the conventional circular pier. However, the scour depth increased with an increase in skewness. Above the 30° skew angle, the modified-shaped piers lost their efficacy due to the increased effective width to the approach flow. In tandem arrangements, replacing a circular pier with a modified-shaped pier showed a decrease in scour depth but the scour reduction depends on pier shape, orientation, and clear spacing between the piers. These results aid decisions on the pier shapes for new bridges near existing ones with circular piers, considering their orientation. The sediment size (d_{50}/D), flow depth (h/D), flow intensity (V/V_c), pier shape factor (K_s), pier aspect ratio (L/D), skew angle (α), and pier spacing (X/D) are used to develop the M5 models. These models accurately predict the maximum scour depth (h_s/D) of isolated and tandem piers. For isolated piers, the M5 models outperform the five regression equations, offering greater reliability. The sensitivity analysis showed that α and V/V_c are the most influential parameters for predicting scour depth around isolated and tandem piers, respectively. This study can be extended to more complex bridge pier geometries, such as non-uniform piers and those with piled foundations.

5. Declarations

5.1. Author Contributions

Conceptualization, S.K.R. and V.C.; methodology, S.K.R. and V.C.; software, S.K.R.; validation, S.K.R., S.T.K., and V.C.; formal analysis, S.K.R. and S.T.K.; investigation, S.K.R.; resources, V.C.; data curation, S.K.R.; writing—original draft preparation, S.K.R.; writing—review and editing, S.K.R., S.T.K., and V.C.; visualization, S.K.R.; supervision, V.C.; project administration, V.C.; funding acquisition, V.C. All authors have read and agreed to the published version of the manuscript.

5.2. Data Availability Statement

The data presented in this study are available on request from the corresponding author.

5.3. Funding

The authors received no financial support for the research, authorship, and/or publication of this article.

5.4. Conflicts of Interest

The authors declare no conflict of interest.

6. References

[1] Choudhury, J. R., & Hasnat, A. (2015, August). Bridge collapses around the world: Causes and mechanisms. IABSE-JSCE joint conference on advances in bridge engineering-III, 21-22 August, 2015, Dhaka, Bangladesh.

[2] Najafzadeh, M., & Oliveto, G. (2021). More reliable predictions of clear-water scour depth at pile groups by robust artificial intelligence techniques while preserving physical consistency. Soft Computing, 25, 5723-5746. doi:10.1007/s00500-020-05567-3.

[3] Kashmoola, A., Ismael, A., & Suleiman, S. (2019). Comparison of Bridge Piers Shapes According to Local Scour Countermeasures. The Eurasia Proceedings of Science Technology Engineering and Mathematics, 6, 171–180.

[4] Oliveto, G., & Hager, W. H. (2005). Further Results to Time-Dependent Local Scour at Bridge Elements. Journal of Hydraulic Engineering, 131(2), 97–105. doi:10.1061/(asce)0733-9429(2005)131:2(97).

[5] Pandey, M., Oliveto, G., Pu, J. H., Sharma, P. K., & Ojha, C. S. P. (2020). Pier scour prediction in non-uniform gravel beds. Water (Switzerland), 12(6), 1696. doi:10.3390/W12061696.

[6] Zarrati, A. R., Gholami, H., & Mashahir, M. B. (2004). Application of collar to control scouring around rectangular bridge piers. Journal of Hydraulic Research, 42(1), 97-103. doi:10.1080/00221686.2004.9641188.

[7] Al-Shukur, A. H. K., & Obeid, Z. H. (2016). Experimental study of bridge pier shape to minimize local scour. International Journal of Civil Engineering and Technology, 7(1), 162-171.

[8] Etemad-Shahidi, A., Bonakdar, L., & Jeng, D. S. (2015). Estimation of scour depth around circular piers: Applications of model tree. Journal of Hydroinformatics, 17(2), 226–238. doi:10.2166/hydro.2014.151.

[9] Fael, C., Lança, R., & Cardoso, A. (2016). Effect of pier shape and pier alignment on the equilibrium scour depth at single piers. International Journal of Sediment Research, 31(3), 244–250. doi:10.1016/j.ijsrc.2016.04.001.

[10] Habib, I. A., Mohtar, W. H. M. W., Elsaiad, A., & El-Shafie, A. (2018). Nose-angle bridge piers as alternative countermeasures for local scour reduction. Baltic Journal of Road and Bridge Engineering, 13(2), 110–120. doi:10.7250/bjrbe.2018-13.405.

[11] Qi, M., Li, J., & Chen, Q. (2016). Comparison of existing equations for local scour at bridge piers: parameter influence and validation. Natural Hazards, 82(3), 2089–2105. doi:10.1007/s11069-016-2287-z.

[12] Sabbagh-Yazdi, S.-R., & Bavandpour, M. (2021). Introducing ring collars and effective spiral threading elevation for cylindrical pier scour control. Marine Georesources & Geotechnology, 40(6), 639–654. doi:10.1080/1064119x.2021.1922555.

[13] Abdulkathum, S., Al-Shaikhli, H. I., Al-Abody, A. A., & Hashim, T. M. (2023). Statistical Analysis Approaches in Scour Depth of Bridge Piers. Civil Engineering Journal (Iran), 9(1), 143–153. doi:10.28991/CEJ-2023-09-01-011.

[14] Baranwal, A., Shankar Das, B., & Setia, B. (2023). A comparative study of scour around various shaped bridge pier. Engineering Research Express, 5(1), 15052. doi:10.1088/2631-8695/acbfa1.

[15] Dargahi, B. (1990). Controlling Mechanism of Local Scouring. Journal of Hydraulic Engineering, 116(10), 1197–1214. doi:10.1061/(asce)0733-9429(1990)116:10(1197).

[16] Huda, M. B., Lone, M. A., Rather, N. A., & Chadee, A. A. (2023). Scouring around different shapes of bridge pier. Water Practice and Technology, 18(7), 1608–1616. doi:10.2166/wpt.2023.108.

[17] Chiew, Y. (1992). Scour Protection at Bridge Piers. Journal of Hydraulic Engineering, 118(9), 1260–1269. doi:10.1061/(asce)0733-9429(1992)118:9(1260).

[18] Li, J., & Tao, J. (2015). Streamlining of Bridge Piers as Scour Countermeasures Optimization of Cross Sections. Transportation Research Record, 2521(1), 162–171. doi:10.3141/2521-17.

[19] Vijayasree, B. A., Eldho, T. I., Mazumder, B. S., & Ahmad, N. (2019). Influence of bridge pier shape on flow field and scour geometry. International Journal of River Basin Management, 17(1), 109–129. doi:10.1080/15715124.2017.1394315.

[20] Laursen, E. M., & Toch, A. (1956). Scour around bridge piers and abutments. Iowa Highway Research Board, Iowa City, United States.

[21] Farooq, R., & Ghumman, A. R. (2019). Impact assessment of pier shape and modifications on scouring around bridge pier. Water (Switzerland), 11(9), 1761. doi:10.3390/w11091761.

[22] Keshavarz, A., Vaghefi, M., & Ahmadi, G. (2022). Effect of the Shape and Position of the Bridge Pier on the Bed Changes in the Sharp 180-Degree Bend. Iranian Journal of Science and Technology - Transactions of Civil Engineering, 46(3), 2449–2467. doi:10.1007/s40996-021-00787-5.

[23] Ismael, A., Gunal, M., & Hussein, H. (2015). Effect of Bridge Pier Position on Scour Reduction According to Flow Direction. Arabian Journal for Science and Engineering, 40(6), 1579–1590. doi:10.1007/s13369-015-1625-x.

[24] Melville, B. W. (1997). Pier and Abutment Scour: Integrated Approach. Journal of Hydraulic Engineering, 123(2), 125–136. doi:10.1061/(asce)0733-9429(1997)123:2(125).

[25] National Academies of Sciences, Engineering, and Medicine. (2011). Evaluation of Bridge Scour Research: Pier Scour Processes and Predictions. The National Academies Press, Washington, United States. doi:10.17226/22886.

[26] Habibi, K., Fard, F. E., Pari, S. A. A., & Shafai-Bejestan, M. (2024). Experimental and theoretical study of sediment scour around angled bridge piers. Canadian Journal of Civil Engineering. doi:10.1139/cjce-2023-0277.

[27] Hoffmans, G. J. C. M., & Verheij, H. J. (2009). Scour Manual. Routledge, London, United Kingdom. doi:10.1201/9780203740132.

[28] do Carmo, J. A. (2005). Experimental study on local scour around bridge piers in rivers. WIT Transactions on Ecology and the Environment, 83. doi:10.2495/RM050011.

[29] Ahmad, N., Melville, B., Mohammad, T., Ali, F., & Yusuf, B. (2016). Clear-water scour at long skewed bridge piers. Journal of the Chinese Institute of Engineers, 40(1), 10–18. doi:10.1080/02533839.2016.1259021.

[30] Raudkivi, A. J. (1986). Functional Trends of Scour at Bridge Piers. Journal of Hydraulic Engineering, 112(1), 1–13. doi:10.1061/(asce)0733-9429(1986)112:1(1).

[31] Melville, B. W., & Sutherland, A. J. (1988). Design Method for Local Scour at Bridge Piers. Journal of Hydraulic Engineering, 114(10), 1210–1226. doi:10.1061/(asce)0733-9429(1988)114:10(1210).

[32] Richardson, E. V., & Davis, S. R. (2001). Evaluating scour at bridges (No. FHWA-NHI-01-001). Federal Highway Administration, Office of Bridge Technology, Washington, United States.

[33] Chiew, Y. M. (1984). Local scour at bridge piers. PhD Thesis, University of Auckland, Auckland, New Zealand.

[34] Abudallah Habib, I., Wan Mohtar, W. H. M., Muftah Shahot, K., El-Shafie, A., & Abd Manan, T. S. B. (2021). Bridge failure prevention: An overview of self-protected pier as flow altering countermeasures for scour Protection. Civil Engineering Infrastructures Journal, 54(1), 1–22. doi:10.22059/CEIJ.2020.292296.1627.

[35] Melville, B. (2008, November). The physics of local scour at bridge piers. Fourth International Conference on Scour and Erosion, 5-7 November, 2008, Tokyo, Japan.

[36] Ettema, R., Mostafa, E. A., Melville, B. W., & Yassin, A. A. (1998). Local Scour at Skewed Piers. Journal of Hydraulic Engineering, 124(7), 756–759. doi:10.1061/(asce)0733-9429(1998)124:7(756).

[37] Fenocchi, A., & Natale, L. (2016). Using Numerical and Physical Modeling to Evaluate Total Scour at Bridge Piers. Journal of Hydraulic Engineering, 142(3). doi:10.1061/(asce)hy.1943-7900.0001096.

[38] Peng Yu, & Zhu, L. (2020). Numerical simulation of local scour around bridge piers using novel inlet turbulent boundary conditions. Ocean Engineering, 218, 108166. doi:10.1016/j.oceaneng.2020.108166.

[39] Shen, H. W., Schneider, V. R., & Karaki, S. (1969). Local Scour Around Bridge Piers. Journal of the Hydraulics Division, 95(6), 1919–1940. doi:10.1061/jyceaj.0002197.

[40] Hancu, S. (1971). On the calculation of local scours in the area of bridge piers. Proceedings of the 14th IAHR congress, 29 August-3 September, 1971, Paris, France. (In French).

[41] Sheppard, D. M., Odeh, M., & Glasser, T. (2004). Large Scale Clear-Water Local Pier Scour Experiments. Journal of Hydraulic Engineering, 130(10), 957–963. doi:10.1061/(asce)0733-9429(2004)130:10(957).

[42] Breusers, H. N. C., Nicollet, G., & Shen, H. W. (1977). Erosion locale autour des piles cylindriques. Journal of Hydraulic Research, 15(3), 211–252. doi:10.1080/00221687709499645.

[43] Heza, Y. B. M., Soliman, A. M., & Saleh, S. A. (2007). Prediction of the scour hole geometry around exposed bridge circular-pile foundation. Journal of Engineering and Applied Science-Cairo, 54(4), 375.

[44] Richardson, J. E., & Panchang, V. G. (1998). Three-Dimensional Simulation of Scour-Inducing Flow at Bridge Piers. Journal of Hydraulic Engineering, 124(5), 530–540. doi:10.1061/(asce)0733-9429(1998)124:5(530).

[45] Kumar, V., Baranwal, A., & Das, B. S. (2024). Prediction of local scour depth around bridge piers: modelling based on machine learning approaches. Engineering Research Express, 6(1), 15009. doi:10.1088/2631-8695/ad08ff.

[46] Quinlan, J. R. (1992). Learning with continuous classes. 5th Australian joint conference on artificial intelligence, 16-18 November, 1992, Hobart, Australia.

[47] Pal, M., Singh, N. K., & Tiwari, N. K. (2012). M5 model tree for pier scour prediction using field dataset. KSCE Journal of Civil Engineering, 16(6), 1079–1084. doi:10.1007/s12205-012-1472-1.

[48] Hassan, Z. F., Karim, I. R., & Al-Shukur, A. H. K. (2020). Effect of interaction between bridge piers on local scouring in cohesive soils. Civil Engineering Journal (Iran), 6(4), 659–669. doi:10.28991/cej-2020-03091498.

[49] Khaple, S., Hanmaiahgari, P., & Dey, S. (2014). Studies on the effect of an upstream pier as a scour protection measure of a downstream bridge pier. River Flow 2014, 2047–2052, CRC Press, Boca Raton, United States. doi:10.1201/b17133-273.

[50] Amini Baghbadorani, D., Beheshti, A. A., & Ataie-Ashtiani, B. (2017). Scour hole depth prediction around pile groups: review, comparison of existing methods, and proposition of a new approach. Natural Hazards, 88(2), 977–1001. doi:10.1007/s11069-017-2900-9.

[51] Hosseini, R., & Amini, A. (2015). Scour depth estimation methods around pile groups. KSCE Journal of Civil Engineering, 19(7), 2144–2156. doi:10.1007/s12205-015-0594-7.

[52] Keshavarzi, A., Shrestha, C. K., Melville, B., Khabbaz, H., Ranjbar-Zahedani, M., & Ball, J. (2018). Estimation of maximum scour depths at upstream of front and rear piers for two in-line circular columns. Environmental Fluid Mechanics, 18(2), 537–550. doi:10.1007/s10652-017-9572-6.

[53] Khaple, S., Hanmaiahgari, P. R., Gaudio, R., & Dey, S. (2017). Interference of an upstream pier on local scour at downstream piers. Acta Geophysica, 65(1), 29–46. doi:10.1007/s11600-017-0004-2.

[54] Selamoğlu, M. (2015). Modeling temporal variation of scouring at dual bridge piers. Ph.D. Thesis, Middle East Technical University, Ankara, Turkey.

[55] Ravanfar, S. M., Mohammadpour, R., & Sabzevari, T. (2023). Experimental study of local scour around non-uniform twin piers. International Journal of River Basin Management, 2023, 1–16. doi:10.1080/15715124.2023.2167823.

[56] Elliott, K. R., & Baker, C. J. (1985). Effect of Pier Spacing on Scour Around Bridge Piers. Journal of Hydraulic Engineering, 111(7), 1105–1109. doi:10.1061/(asce)0733-9429(1985)111:7(1105).

[57] Ataie-Ashtiani, B., & Beheshti, A. A. (2006). Experimental Investigation of Clear-Water Local Scour at Pile Groups. Journal of Hydraulic Engineering, 132(10), 1100–1104. doi:10.1061/(asce)0733-9429(2006)132:10(1100).

[58] Liu, M. ming, Wang, H. cheng, Tang, G. qiang, Shao, F. fei, & Jin, X. (2022). Investigation of local scour around two vertical piles by using numerical method. Ocean Engineering, 244, 110405. doi:10.1016/j.oceaneng.2021.110405.

[59] Dey, S., & Sarkar, A. (2006). Scour Downstream of an Apron Due to Submerged Horizontal Jets. Journal of Hydraulic Engineering, 132(3), 246–257. doi:10.1061/(asce)0733-9429(2006)132:3(246).

[60] Yang, Y., Melville, B. W., Macky, G. H., & Shamseldin, A. Y. (2019). Local scour at complex bridge piers in close proximity under clear-water and live-bed flow regime. Water (Switzerland), 11(8), 1530. doi:10.3390/w11081530.

[61] Ettema, R. (1980). Scour at Bridge Piers. Ph.D. Thesis, University of Auckland, Auckland, New Zealand.

[62] Neill, C.R. (1967) Mean Velocity Criterion for Scour of Coarse Uniform Bed Material. Proceeding of the 12th Congress of the International Association of Hydraulics Research, 11-14 September, 1967, Colorado State University, Fort Collins, United States.

[63] Raudkivi, A. J., & Ettema, R. (1983). Clear-Water Scour at Cylindrical Piers. Journal of Hydraulic Engineering, 109(3), 338–350. doi:10.1061/(asce)0733-9429(1983)109:3(338).

[64] Ettema, R., Melville, B. W., & Barkdoll, B. (1998). Scale Effect in Pier-Scour Experiments. Journal of Hydraulic Engineering, 124(6), 639–642. doi:10.1061/(asce)0733-9429(1998)124:6(639).

[65] Jayaraman, S. (1995). Hydraulic modelling. Indian institute of Technology Madras, Chennai, India.

[66] Dey, S. (2014). Fluvial Hydrodynamics. GeoPlanet: Earth and Planetary Sciences. Springer, Berlin, Germany. doi:10.1007/978-3-642-19062-9.

[67] Alipour, A., Yarahmadi, J., & Mahdavi, M. (2014). Comparative Study of M5 Model Tree and Artificial Neural Network in Estimating Reference Evapotranspiration Using MODIS Products. Journal of Climatology, 1–11. doi:10.1155/2014/839205.

[68] Etemad-Shahidi, A., & Ghaemi, N. (2011). Model tree approach for prediction of pile groups scour due to waves. Ocean Engineering, 38(13), 1522–1527. doi:10.1016/j.oceaneng.2011.07.012.

[69] Mia, M. F., & Nago, H. (2003). Design Method of Time-Dependent Local Scour at Circular Bridge Pier. Journal of Hydraulic Engineering, 129(6), 420–427. doi:10.1061/(asce)0733-9429(2003)129:6(420).

[70] Sheppard, D. M., Demir, H., & Melville, B. W. (2011). Scour at wide piers and long skewed piers. Transportation Research Board, Washington, United States.

[71] Mostafa, E. A. (1994). Scour around skewed bridge piers. Alexandria University, Alexandria, Egypt.

[72] Moussa, A. M. A. (2018). Evaluation of local scour around bridge piers for various geometrical shapes using mathematical models. Ain Shams Engineering Journal, 9(4), 2571–2580. doi:10.1016/j.asej.2017.08.003.

[73] Liang, D., Gotoh, H., Scott, N., & Tang, H. (2013). Experimental Study of Local Scour around Twin Piles in Oscillatory Flows. Journal of Waterway, Port, Coastal, and Ocean Engineering, 139(5), 404–412. doi:10.1061/(asce)ww.1943-5460.0000192.

[74] Wang, H., Tang, H., Liu, Q., & Wang, Y. (2016). Local Scouring around Twin Bridge Piers in Open-Channel Flows. Journal of Hydraulic Engineering, 142(9), 06016008. doi:10.1061/(asce)hy.1943-7900.0001154.

[75] Wang, Y., & Witten, I. H. (1996). Induction of model trees for predicting continuous classes. Working paper 96/23, The University of Waikato, Hamilton, New Zealand.

[76] Pasha, M. M., Mahmood, A. H., & Shams, S. (2016). An analysis of scouring effects on various shaped bridge piers. Brunei Darussalam Journal of Technology and Commerce, 29-42.

[77] Talib, A., Obeid, Z. H., & Hameed, H. K. (2016). New imperial equation for local scour around various bridge piers shapes. International Journal of Science and Research (IJSR), 5(9), 654-658.

[78] Chabert, J., & Engeldinger, P. (1956). Study of Scour at Bridge Piers. Bureau Central d'Etudes les Equipment d'Outre-Mer, Laboratoire National d'Hydraulique, Chatou, France.

[79] Bhattacharya, B., Price, R. K., & Solomatine, D. P. (2007). Machine Learning Approach to Modeling Sediment Transport. Journal of Hydraulic Engineering, 133(4), 440–450. doi:10.1061/(asce)0733-9429(2007)133:4(440).

[80] Beg, M. (2004). Mutual interference of bridge piers on local scour. Proceedings of the Second International Conference on Scour and Erosion, 14-17 November, 2007, Singapore.

[81] Devi, G., & Kumar, M. (2022). Experimental study of the local scour around the two piers in the tandem arrangement using ultrasonic ranging transducers. Ocean Engineering, 266, 112838. doi:10.1016/j.oceaneng.2022.112838.

[82] Liang, F., Wang, C., Huang, M., & Wang, Y. (2017). Experimental observations and evaluations of formulae for local scour at pile groups in steady currents. Marine Georesources and Geotechnology, 35(2), 245–255. doi:10.1080/1064119X.2016.1147510.

[83] Malik, R., & Setia, B. (2021). Local scour around closely placed bridge piers. ISH Journal of Hydraulic Engineering, 27(4), 396–403. doi:10.1080/09715010.2018.1559772.

[84] Yang, Y., Qi, M., Wang, X., & Li, J. (2020). Experimental study of scour around pile groups in steady flows. Ocean Engineering, 195, 106651. doi:10.1016/j.oceaneng.2019.106651.